REPORT

Verification calculation IJssel bridge A12

Main bridges

Customer: Rijkswaterstaat

Reference: T & P-BF7387-R004-F2.0

Status: 2.0 / Final

Date: March 23, 2020

Page 2

Project related

HASKONINGDHV NEDERLAND BV

Box 151
6500 AD Nijmegen
Transport & Planning
Trade register number: 56515154

+31 88 348 70 00 T
+31 24 323 93 46 F
info@rhdhv.com E
royalhaskoningdhv.com W.

Title document: Verification calculation IJssel bridge A12

Subtitle: Verification calculation Hoofdbruggen
Reference: T & P-BF7387-R004-F2.0
Status: 2.0 / Final
Date: March 23, 2020
Project name: Recalculation and reinforcement design IJsselbrug A12
Project number: BF7387
Author (s): E. Klamer, N. Elbers, A. Akyel

Prepared by: E. Klamer, N. Elbers, A. Akyel

Checked by: Rob Soetekouw

Date / initials: 3/23/2020

Approved by: Karel Vis

Date / initials: 3/23/2020

Classification

Project related

Project related

Content

Project related

Project related

Project related

Project related

Project related

Attachments

Appendix A Taxes

Appendix B Modeling

Appendix C Assessment of strength and stability

Appendix D Assessment of connections

Appendix E Fatigue assessment

Project related

Version	Adjustment	Date
D0.1	First draft, for assessment (internal) (H1 to H4)	08/23/2018
D0.2	Second draft, for assessment (internal) (H1 to H4)	9/5/2018
D0.3	Third concept, internal testing processed, for verification to RWS (H1 to H4)	9/17/2018
D0.4	Fourth draft, for assessment (internal) (H5 to H7)	9/17/2018
D0.5	Fifth concept, internal assessment processed, for verification to RWS (H5 to H7)	10/26/2018
D0.6	Sixth draft, RWS comments processed. for assessment (internal)	1/28/2019
F1.0	First Final version	2/12/2019
F1.1	- Lower flange stability test adjusted from tilt test to kink test (§3.1.6) - Tested torsion stability longitudinal stiffeners corrected (formula λ_s) (§3.1.7) - Verification of vertical portals adjusted based on the progressive normal force (§3.3) - Analysis of normal force vertical movements added (§3.3.4) - Error in damage calculation type H2 corrected (§5.10)	5/2/2019
F1.2	Addition that all couplings of the section divisions have to be replaced (§4.8 and §8.2) Addition of fatigue through coupling lower longitudinal stiffener at portal C (§5.21)	5/27/2019
F1.3	Mortar plate fatigue test added (§5.22)	7/24/2019
F2.0	References TNO / IIW added (§1.1) UGT testing portals with plate model added (§ 3.3.4 to 3.3.6) Fatigue connection crossbars - main beams based on measurements added (§5.19 to 5.25)	3/23/2020

Project related

1 Reading Guide

In this report, the results of the verification calculations of the main bridge (s) of the IJssel bridge A12 treated. This report serves in conjunction with the basic report recalculation IJsselbrug A12 [T & P-BF7387-R001-F1,1] to be read.

Bridge Bridge Main bridge

Figure 1 - Side view of the IJssel bridge [A.46205A]

The basic report includes the materials used, construction phases and loads that are applicable for the calculation of both the main and the bridges. Also in the basic report, the modeling is discussed, including the SCIA input, as well as the verification of the finite element model. These parts will therefore not be included in this report be repeated. Exceptions are the loads, where the loads are specific to the main bridge further elaborated (chapter 2). The support conditions were also checked in this chapter.

Chapter 3 will discuss the strength and stability testing of the various construction parts. Chapter 4 then examines the testing of connections. The results of the fatigue analysis are discussed in chapter 5. In chapter 6 the deformation of the joint transitions and the supports. Chapter 7 will then be discussed on the consequences of the acceptance tax. In chapter 8 the results are summarized and, if necessary, made recommendations for further research and / or reinforcements.

1.1 References

In addition to the references in the basic report, the following reports have been used for the verification calculations:

[1] TNO Report TNO-2017-R11499. Various fatigue advice for the bridge near Rheden, 2017
[2] TNO Note 100315818 / ALL. Fatigue classification of fillet welds in crotch and T-joints. 2018
[3] TNO Report TNO-2018-R11423. Fatigue IJssel bridge Rheden - not absorbing force rivets, 2018
[4] TNO Report TNO-2018-R10290B. Description of preventive emergency repairs for the bridge at Rheden, 2018
[5] TNO Memorandum 0100313038-A / VSS. Detail categories and inspection intervals after

reinforcements at the bridge near Rheden, 2018
[6] TNO Report TNO-2019-R11393. Rack measurements IJsselbrug, 2019
[7] TNO Report TNO-2019-R11394. Various advice on fatigue life
crossbeam connections IJsselbrug, 2020
[8] TNO Report TNO-2019-R10527. Risk analysis of welding imperfections in the IJsselbrug A12, 2019
[9] TNO Report TNO-2020-R10226. Rack measurements IJsselbrug, 2020
[10] IIW Document IIW-2259-15 ex XIII-2460-13 / XV-1440-13. Recommendations for Fatigue Design of Welded Joints and Components, 2016
[11] IIW-Doc. XIII-2380r3-11 / XV-1383r3-11. IIW Guideline for the Assessment of Weld Root Fatigue, 2012

Project related

2 Modeling

The modeling of the main bridge is covered in the basic report. Additions to this are in this chapter.

2.1 Taxes

The taxes for the IJssel Bridge have been dealt with in the basic report. Both discussed here the loads on the main and the bridges. In Appendix A , the loads of the main bridge further elaborated for the input in the calculation models in SCIA Engineer.

The different taxes are shown in the following appendices:

Appendix A1 : Permanent taxes
Appendix A2 : Traffic taxes
Appendix A3 : Wind load
Appendix A4 : Temperature load
Annex A5 : Other loads (hot water pipe and acceptance load)

The input of the taxes and tax combinations in the SCIA model is shown in Appendix B1 for the global model and Appendix B2 for the local model. The tax input has been verifi control of the resultants, see Appendix B3 for the global model and Appendix B4 for th

2.2 Influence of the inspection on the modeling

For discussion and explanation of the results of the inspection, reference is made to report T&P-BF7387-R009. No significant defects were found during the inspection, such an influence have on the modeling of the bridge. Detected material removal from the main supporting structure was found to be less than 5% in all cases. For example, the consoles show superficial corrosion, but remain this corrosion is limited in cross-section decrease.

Figure 2 - Corrosion connection inspection paths on deck construction edge.

Project related

However, the joints of the inspection paths show considerable corrosion. It is recommended to do this to replace. However, this has no consequences for the modeling of the main supporting structure.

Figure 3 - Corrosion connection inspection paths on deck construction edge.

It has also been found that the first diagonal of the river span is bent on one side. It is unclear what exactly happened, this may have happened during an earlier inspection of the bridge due to collision with a man lift on a boat or a man lift. It is recommended to take this with you with major maintenance. However, this has not been included for modeling.

Figure 4 - Distortion of the diagonal of one of the diagonals in the river span.

The geometry of the construction also appears to correspond to the drawings. The construction is then also modeled in accordance with the design drawings. However, connections A5, B4 and B7 are in the main carriageway west, modifications to the connection have been carried out, see TNO report [2018 R10290B]. This has however, no consequences for the modeling.

Project related

3 Strength and stability

3.1 Main beam

3.1.1 Calculation approach

To determine the normative cross sections for the assessment of the main beams are in the first instance the Von Mises voltages (based on the Huber Hencky yield criterion) determined using SCIA Engineer (see also Appendix C1 .a). In the figures below, the Von Mises stresses are in the main beam of the UGT envelope shown for the first 3 fields.

npoint G

Steu

Figure 5 - Von Mises tensions main girders field 1 (UGT)

Figure 6 - Von Mises stresses of main beams in field 2 (UGT)

Project related

.4

npoint H

Field 3

Steu

Connection A

Figure 7 - Von Mises stresses of main beams in field 3 (UGT)

Different jumps are visible in the tensions. These are caused by transitions in the cross-section of the bottom flange and / or cover plate thickness. In addition, small peaks are visible that are rising towards the crossbars. These are caused by the moment about the weak axis (M_z).

This can be seen, in particular at the support points G and H, the middle of the river span

(field 3) and the highest voltages occur near connection A.4. The Von Mises tensions are up support point H, the center of the river span and near connection A.4 higher than the permissible yield stress of 350 N / mm².

In the SCIA calculation of the Von Mises stresses, moments around the weak axis (M_z) are also taken away. However, the calculation of M_z will not be correct because:

- The main beam for transverse bending will not be dimensionally stable, due to the relatively flexible, high body. Only the lower part of the main beam is relevant for cross bending. The top flange is namely connected to the deck. As a result, the transverse stiffness (I_z) will not be correct and so will it $M_{z\,are}$ not correct.
- In addition, the vertical stiffeners and the K-bandage in the model are not connected to the lower flange of the main beam, because beam elements have been used for the main beams. The vertical stiffeners and the K-bandages will ensure that the loads in the transverse direction on the main beam is transferred directly to the deck.
- In addition, the beam element is not at the correct height to correct the transverse bending that occurs modeling, the purpose of the model is to model the bend around the strong axis correctly, so that the center of gravity is correct only for the longitudinal direction.

The magnitude of transverse bending stress has been examined in chapter 5.2, where the stress by transverse bending due to a unit load of 2x50 kN for the fatigue calculations a local model with plate elements. This tension in the lower flange was found to be a maximum of 0.7 N / mm². This is therefore approximately 4 N / mm² for a tandem system of 600 kN. For the substantiation of this is refer to chapter 5.2.

The extra tension this gives will only very limited extra pressure and pull in the bottom flange. because of this the flange on one side will flow a little earlier, but the stretch on the smooth side will be limited by the printed other side of the bottom flange that does not flow. As a result, the flow stretches will be very limited well within the allowable yield strength limit.

In consultation with Rijkswaterstaat, it was decided to take the time to consider the weak axis for the strength calculation neglect.

Project related

3.1.2 Results

In the figures below, the tension in the top and bottom flange are due to the normal force (N_{Ed}) plus the moment about the strength axis ($M_{y,Ed}$) displayed for half of the bridge. For the top flange is based on the flange of the eccentric beam, this corresponds to the bottom of the deck. For the calculation of the stresses in the deck, see paragraph 3.4 .

Top flange tension (ULS)

350
300

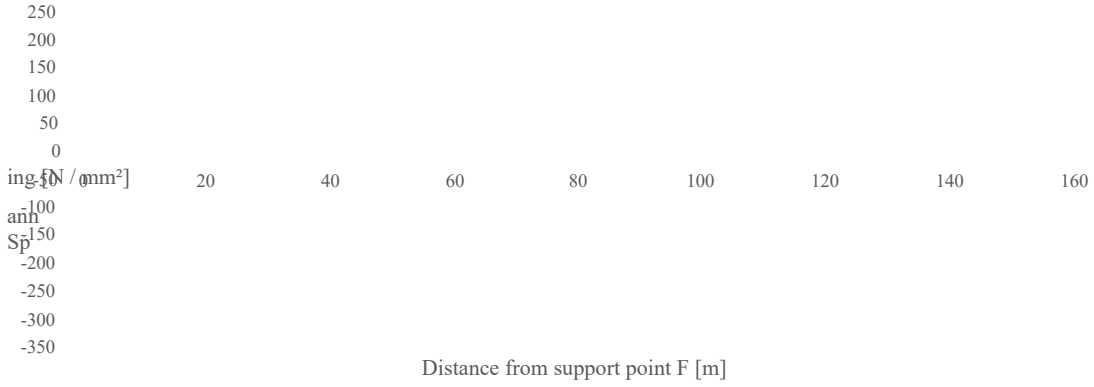

Figure 8 - Top flange stress due to N Ed + M y, Ed main beams (UGT)

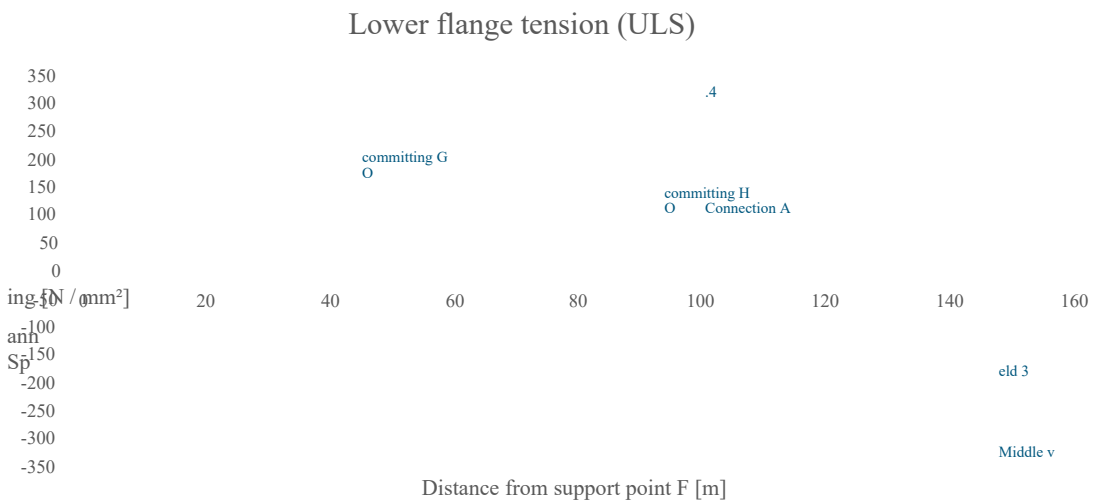

Figure 9 - Lower flange stresses due to N Ed + M y, Ed main beams (UGT)

It can be seen that the stresses remain below the yield point of 350 N / mm².

Project related

In the figures below, the tension is in the top and bottom flanges of the individual load components shown along the length of the half bridge (without load factor).

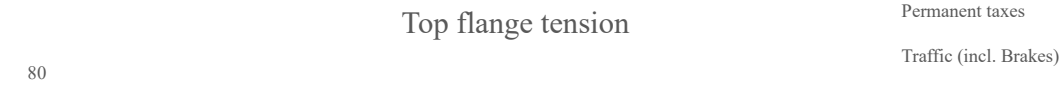

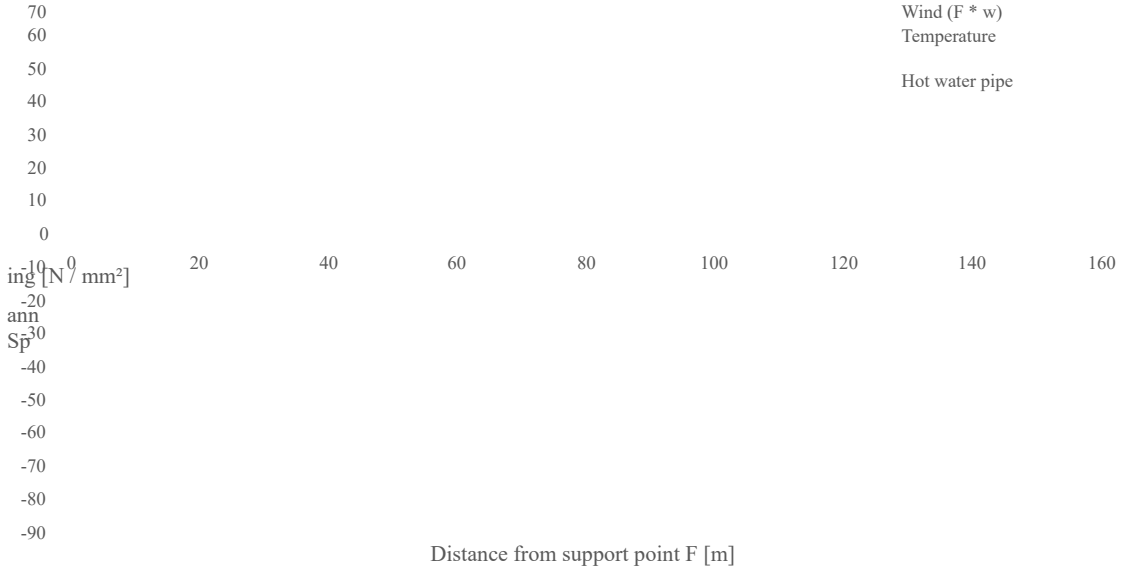

Figure 10 - Stresses top flange main beams due to $N_{Ed} + M_{y,Ek}$ (per load group)

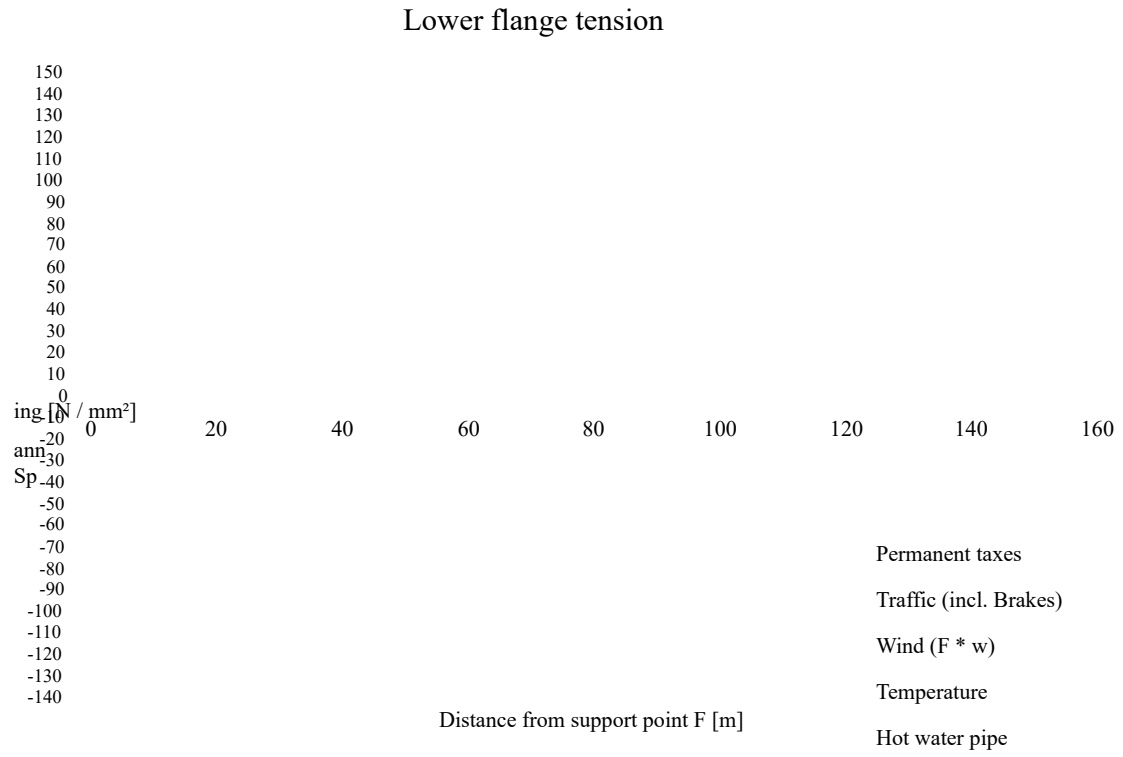

Figure 11 - Stresses lower flange main beams due to $N_{Ed} + M_{y,Ek}$ (per load group)

3.1.3 Calculation approach fold of the body

In the determination of the abovementioned stresses no account has yet been taken of the fold of the main beams and the presence of the stiffeners. The extra longitudinal stiffeners result in something larger cross-section, while pleat ensures that calculations must be made with a reduced one intersection. That is why fold calculations of four were made with Mathcad design cuts, as shown in Figure 9 , where both the additional longitudinal stiffeners and the reduced effective cross-section for the bending test have been included. Then based on the results are examined to see whether it is necessary to test even more cuts. The calculations are shown in Appendix C1 .b to f. The cutting forces of the tested cuts are shown in Appendix C1 .a.

The following components have been tested in the fold calculations, in accordance with NEN-EN 1993-1-5:

- Gross cross-section assessment (excluding pleat stiffeners)
- Test effective cross section (including pleat stiffeners)
    - o Resistance to normal voltages (due to bending)
    - o Shear resistance (due to shear force)
    - o Interaction between shear and bending moment
- Testing stiffeners and detailing
    - o Check rigid or deformable transverse stiffeners with regard to normal stresses
    - o Check rigid or deformable transverse stiffeners with regard to shear
    - o Check rigid or deformable stiffening on the support
- Assessment of folds caused by the flange

The above tests were performed for the four normative cuts, as in the following figures.

G-1

Figure 12 - Section G-1 [A.85363]

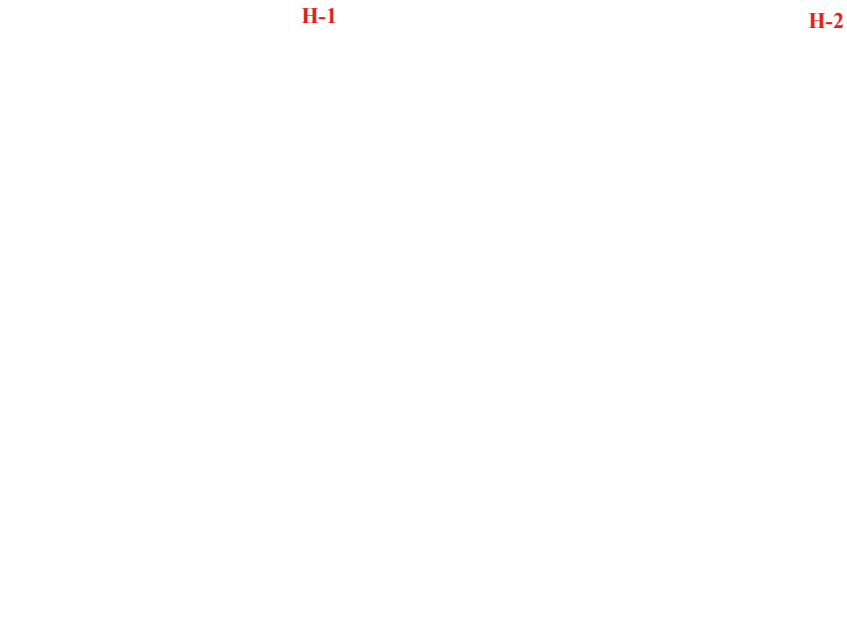

Figure 13 - Section H-1 and H-2 [A.85365]

Figure 14 - Section V3-1 (midfield 3 (river span)) [A.85367]

3.1.4 Results fold calculation

From the calculations it follows that the cross stiffeners at the K-bandages as rigid cross stiffeners with regard to normal stresses and shear may be considered. The intermediate transverse stiffeners however, in some cases, deformable cross stiffeners must be used for both normal stresses (H-1, H-2) as shear (H-1, H-2, V3-1). The critical one is for these cases pleat tension of the field between two K-relations determined using EB-plate, so that account is taken can be held with the intermediate flexible cross stiffeners. It has also been established that there is is of a rigid stiffening on the supports.

The test results of the main strength tests are for these four normative sections shown in the table below.

Cut	Location dx [mm]	Voltage obv class 3 [N / mm²]	Voltage obv class 4 [N / mm²]	UC normal-tensions due to bending	UC shear	UC shear force and bending	UC folds causes through flange
G-1	44996	-246	-249	0.71	0.62	0.73	0.46
H-1	95015	-313	-325	0.93	0.61	0.74	0.68
H-2	100953	-337	-357	1.02	0.55	0.60	0.49
V3-1	147525	343	343	0.98	0.14	0.98	0.30

Table 1 - Overview of unity checks for bending assessment of main beam (UGT)

It should be noted that the tension based on class 3 is carried out without the longitudinal stiffeners, while the assessment based on class 4 with longitudinal stiffeners has been carried out.

For the assessment of "folds caused by the flange" it is assumed that folds occur in the web plate between the flange and the second longitudinal stiffener, without taking into account the support of the first longitudinal stiffener. In reality, crease will occur between the bottom flange and the first longitudinal stiffener, but because it may not be fully considered rigid support based on the height between the pressed flange and the second longitudinal stiffener. In the calculation is takes into account the curvature of the bottom flange.

It turns out that only the cut H-2, at connection A.4, just does not satisfy the fold due to longitudinal stresses. That is why it was checked for this cut whether the cross-section complies with the reduced wind load and reduced tax combinations, as described in the basic report (section 6.4 and 6.9). If the bending test is performed with these reduced cutting forces, the cross section (see Appendix C1.f).

Cut	Location dx [mm]	Voltage based on class 3 [N / mm²]	Voltage based on class 4 [N / mm²]	UC normal-tensions due to bending	UC shear	UC shear force and bending	UC folds causes through flange
H-2	100953	-320	-338	0.97	0.52	0.59	0.49

Table 2 - Overview of unity checks for bending check of main beam (reduced load combinations)

The calculations show that the increase in stresses due to the cross section reduction method maximum 20 N / mm². The height of the most printed plate field is relatively constant in height length of the bridge. In the fields this is always 900 mm (top), at the support points 700 mm (bottom). On this basis, the degree of stiffening against folds along the length of the bridge will be comparable. The increase in tension after taking the cross-section reduction into account will occur in other cuts therefore not increase much more than the 20 N / mm² calculated here. The maximum pressure in field 1 is -143 N / mm² (top flange), in field 2 maximum -244 N / mm² (bottom flange). Even after charging of the cross-section reduction, the stresses in these fields will be (more than) lower than the yield strength of 350 N / mm². These cuts have therefore not been tested further.

3.1.5 Body wind load

Tensions due to wind load have not yet been taken into account in the calculation of the main beam perpendicular to the body. The wind load must be transferred to the stiffeners via the web plate and then to the K-bandages and the deck. The size was determined using the local model of the stresses in the web plate and the pleat stiffeners due to the wind load.

*Figure 15 - Stresses in web plate and pleat stiffeners due to wind load F * w (seen from the inside of the bridge)*

It can be seen that the stresses in the web plate in the outer fields are a maximum of 3 N / mm², which corresponds to a manual calculation of these voltages. Tensions run in the larger fields a little further up to a maximum of 5 N / mm², but here the stresses due to bending will not be maximum. Tensions of up to 5 N / mm² are also found in the pleat stiffeners. Considering the low tensions it is justifiable to neglect these in the calculation.

3.1.6 Stability

Buckling of the bottom flange

In addition to the strength calculation, stability of the bottom flange (kinking out of plane) was checked. The cross stiffeners at the intermediate cross bars are not able to provide sufficient support against it buckling of the bottom flange. Therefore, a buckling length corresponding to the length has been assumed between the K-relationships. The test was carried out in accordance with Article 6.3.1, whereby the bottom flange is considered a printed bar. When determining the surface area and the moment of inertia based on the surface of the bottom flange plus 1/3 of the (effective) parts of the body under pressure. The longitudinal stiffeners on pressure are also included for 1/3. The calculation is shown in the Mathcad calculations where the bend tests are also performed, because the effective part of the body must be included in the calculation. Please refer to Appendix C1 for this. The results of the kinks are summarized in the table below.

Cut	Location dx [mm]	UC
G-1	44996	0.71
H-1	95015	0.93
H-2	100953	1.03 (0.97) [1]

[1] *reduced tax combinations*

Table 3 - Overview of unity checks for stability of the lower flange of the main beam (ULS)

A small overshoot is found for section H2. With the reduced wind load and reduced tax combinations is sufficient. In addition, the calculation is not yet taking into account that an additional flange plate of 550x30 mm is present over the first 700 mm, with afterwards another sloping piece of 650 mm. This gives extra resistance to buckling of the bottom flange present.

3.1.7 Long stiffeners

Get well soon

The longitudinal stiffeners have a lower yield strength (QMc 37) compared to the main beams (LQMc 52). The tension at the 1 st longitudinal stiffener has therefore also been tested for the lower yield stress. Field 3 has not been tested since the longitudinal stiffener is almost in the neutral line.

Cut	Location dx [mm]	Voltage based on class 4 [N / mm²]	UC normal voltages due to bending
G-1	44996	-134	0.62
H-1	95015	-248	1.15
H-2	100953	-279 (-265) 1	1.30 (1.23) 1

1 reduced tax combinations

Table 4 - Overview of unity checks for the tension in the 1 st longitudinal stiffener of the main beam (UGT)

It can be seen that the stresses at section H-1 and H-2 are too high relative to the yield stress (f_y = 215 N / mm²). This will cause the lower longitudinal stiffener to flow into the UGT.

Torsional buckling of the stiffeners

The torsional stiffness of the transverse and longitudinal stiffeners was initially tested against the stiffness criterion in accordance with NEN-EN 1993-1-5 art. 9.2.1 (8). The cross stiffeners meet this requirement, the longitudinal stiffeners not. In this test, the length between the supports is not a parameter, so it is assessment is therefore very conservative. In accordance with the National Annex, the torsion stability can also be demonstrated by complying with art. 13.8.3 of NEN 6771. This does take into account the length of the longitudinal stiffener between the supports. From the calculations it follows that torsional buckling of the longitudinal stiffeners occur at an (equivalent) compressive stress of -189 N / mm². This includes a contribution of the shear stress of approximately 19 N / mm², which means that the normal stress in the longitudinal stiffener maximum -170 N / mm². The calculations are included in the Mathcad calculations of the

fold calculations in Appendix C1.

The figure below shows the tension in the longitudinal stiffeners and the tension where torsional buckling occurs. It can be seen that the stresses at section H-1 and H-2 are too high relative to the stress at which torsional buckling occurs (f_y = -170 N / mm²).

Figure 16 - Tensions in the longitudinal stiffeners and torsional buckling stress (ULS)

Project related

The figure below shows in red in which area the longitudinal stiffener is not sufficient.

Figure 17 - Area where the longitudinal stresses are higher than permissible

It is recommended to replace the longitudinal stiffeners in the specified area, or if the main beam is strengthened in this area for other reasons (eg fatigue), demonstrating that the longitudinal stiffener is sufficient in the reinforced situation.

Project related

3.2 Crossbars

3.2.1 Calculation approach

The crossbars of the main span have been tested against the yield stress criterion. Be for this uses the Von Mises voltages from the local SCIA engineer model; see Appendix C2. Be in this model all relevant taxes are modeled, so that tax effects from the global model are not need to be taken.

The crossbeam has not been tested for buckling and tipping as the bottom flange remains largely on tension and it profile is supported at the top by the steel driving deck. Only at the location of the connection with the main beam creates pressure in the lower flange due to a point of support moment. However, Figure 1 shows that the Von Mises voltages with 90 MPa are relatively low. The same also applies to the console, outside the main beam.

The bottom flange of the cross beam falls into section class 3. The web falls into class 1, The cross beam therefore does not need to be checked for folds.

3.2.2 Results

In the images below, the maximum Von Mises stresses in the design crossbeam displayed. The maximum UGT tension in the cross beam is 240 MPa and occurs in the bottom flange. The normative tax combination is “6.10b gr1a traffic normal”.

The SCIA results show a number of fluxes in a number of places. It goes here however, very local voltage peaks are related to sharp grid elements and are therefore ignored.

The maximum von Mises voltage in the consoles is 120 MPa and occurs in the top of the body.

Figure 18 - Von Mises strains crossbeam

Cut	σ_d [N / mm²]	f_{yd} [N / mm²]	UC
Cross beam - bottom flange	240	350	0.68
Console - top of body	120	350	0.63

Table 5 - Overview of unity checks for strength testing of crossbars

Project related

To gain more insight into the composition of the maximum stresses, Appendix C2 and the table below shows the contributions of the various tax components (without tax factor) summarized.

Load crossbars	Bottom field
	σ_{max} [mPa]
UGT (DD UGT)	240
Permanent taxes	6
Traffic	120

Brake	0
Wind F * w	1
Temperature	21
Hot water pipe	7

Table 6 - Load case results diagonally (in cut outside node)

Project related

3.3 K-bandages and portals

In this chapter, the approach and results of the assessment of the strength and stability of the K-relationships and portals presented. For model output and calculations, see Appendix C3 .

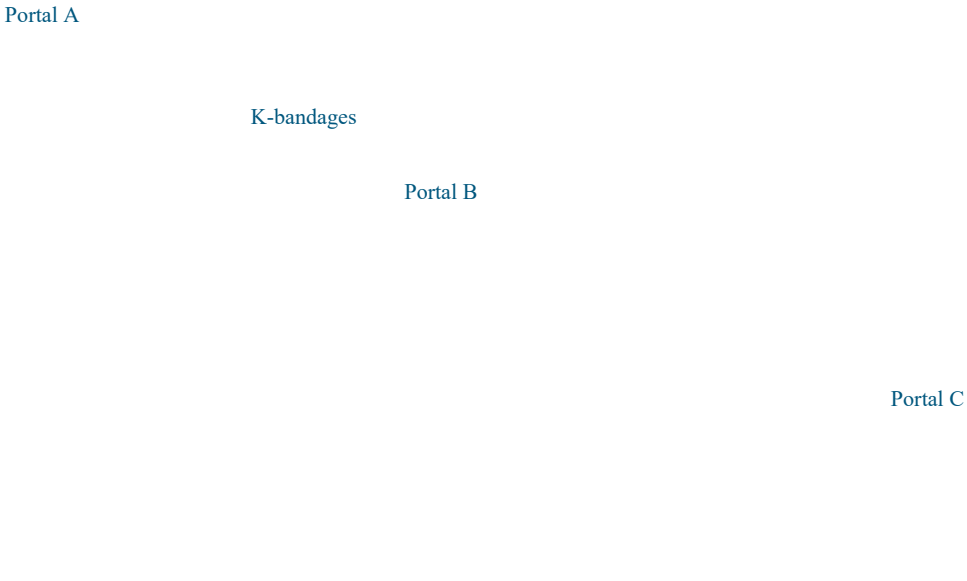

Figure 19 - Location K-bandages and portals

3.3.1 Bar model calculation approach

In the first instance, the results were used to assess the K-relationships and portals of the global bar model. Based on the bar forces from this model, the cross sections are on strength and stability tested. The cross-section assessment was performed with Excel spreadsheets.

Initially, the assessments were based on conservative values for the buckling length factor and interaction factors and is calculated with the maximum forces. If the assessment is not met, the actual values determined and the cut moved from the node to the day of the link.

The contribution of the body of the main girders is the cross-section assessment of the vertical of the portals taken away. Here is a cooperative width on both sides of the profile of $15\varepsilon * t_w$ taken into account, where t_w is counted on the body thickness including thickening plates in the body. For the bend check of the body of the main beam is referred to section 3.1 .

The tensile bearings have been taken into account for testing the lower edge of portal B. In the Calculation model is the on-site imposition of the pressure superimposition, so that it is not a non-linear calculation must be performed. The bottom edge has been manually checked at the moment occurs with a maximum pulling force in the towing support (see section 3.5. 1). The occurring moment is My = 529 kN * 0.85 m = 450 kNm.

3.3.2 Results of K-dressings

All parts of the K-bandages meet strength and stability. The normative UC is 0.66 and perform in a vertical.

Profile diagonals	get well soon	stability
Diagonals 2x L80x8	0.31	0.31
Diagonals 2x L90x9	0.25	0.30
Horizontal 0.5 DIN 20	0.03	0.09
Vertical 0.5 INP24 + 0.5 INP 24	0.59	0.59
Vertical 0.5 INP24 + 0.5 INP 30	0.66	0.66
Vertical 0.5 INP24	0.34	0.34
Vertical 0.5 INP30	0.33	0.33
Vertical L90x9	0.23	0.25

Table 7 - Overview of unity checks K-relationships

3.3.3 Portal results

The table below gives an overview of the UCs of the different parts of the portals.

Location	profile	get well soon	stability
Diagonal portal A	2x L100x10 2LX	0.44	0.60
Diagonal portal B	2x L100x10 2LX	**1.11** / 0.96 [1]	0.95 / 0.79 [1]
Diagonal portal C	2x UNP 260	**1.12** / **1.11** [1] / 0.79 [1,3]	0.96 / 0.95 [1] / 0.83 [1,3]
Bottom and top edge of portal A Horizontals 0.5 DIN 20		0.26	0.37
Bottom edge of portal B	I profile	0.15 / 0.65 [2]	0.22 / 0.41 [2]
Bottom and top edge of portal C 2x UNP 260		**1.20** / **1.19** [1] / 0.98 [1,3]	0.85 / 0.84 [1] / 0.65 [1,3]
Vertical portal A	1/2 INP30 + 1/2 INP30	**1.05** / **1.01** [1] / 1.00 [1,3]	0.86 / 0.80 [1] / 0.79 [1,3]
Vertical portal B	150x12 + 126x12 + 0.5 INP30	**1.82** / **1.69** [1] / **1.59** [1,3]	**1.33** / **1.23** [1] / **1.17** [1,3]
Vertical portal C	composed	**1.02** / 0.98 [1]	**1.04** / 0.99 [1]

[1] reduced wind load and load combination cf. basic report §6.4 and §6.9
[2] load combination pull connection
[3] reduced wind load (CsCd = 0.85 and b / d up to based on the width of two bridges)

Table 8 - Overview of unity checks portals

From the calculation under the normal load combinations it follows that various diagonals, verticals and bottom edges of the portals are not sufficient. That is why it was examined whether these parts are satisfactory under the reduced wind load and load combinations, as described in the basic report, sections 6.4 and 6.9. The UC for these tax combinations is indicated by a subscript [1] . Also with a number of components were found to be unsatisfactory in this combination.

Reduced wind load ($c_s c_d$ = 0.85 and b / d up to two bridges)

In consultation with Rijkswaterstaat, the following optimization has therefore been implemented in the assessment of the portals. There was still some conservatism in determining the wind load. With a separate the assessment was carried out again, with the following issues being adjusted.

- $c_s c_d$ factor in the calculation of the wind load is maintained as 0.85 instead of 1.00
- b / d to ratio in the determination of the wind load is based on the two steel bridges together instead of a single bridge

The calculation of the adjusted wind load is shown in Appendix A3c and d. When the construction is calculated with this adjusted wind load, it appears that only the vertical van portal B is not sufficient. The results are indicated in the table above with a subscript 3 .

To gain insight into the tax shares of the different types of taxes is given below Sections give a breakdown of the stress per load type for the diagonals and verticals of portal B and C (based on the original model without reductions in wind load). The voltage is the maximum value of N_{max} + associated $M_y + M_z$ and M_{ymax} with associated $N + M_z$.

Diagonals

The UC of the diagonals is mainly determined by the normal force and bending around the strong axis.

Load diagonals	Portal B	Portal C
	σ_{max} [mPa]	**σ_{max} [mPa]**
UGT (HL UGT)	-238	-255
BGT (HL cart)	-180	-173
Permanent taxes	-27	-4
Traffic	-86	-17
Brake	-1	0
Wind F * w	-61	-153
Temperature	-11	-2
Hot water pipe	-2	-1

Table 9 - Load case results diagonal (in cut outside node)

It is noted that the profiles are class 1, so the UC cannot be compared one-to-one with the tension. The proportion of normal force in the benchmark test (N_{max}) is approximately 70%. The normal force is in accordance with the original design calculation. Created by wind and traffic bending moments that initially raised the UC above 1.0. This bending moments were not included in the original design calculation. After reduction of the wind load shows that the diagonals are sufficient.

Verticals

The contributions of the different loads to the stresses in the verticals are shown below
table shown (based on the original model without reductions in wind load).

Load verticals	Portal B	Portal C
	σ_{max} [mPa]	σ_{max} [mPa]
UGT (HL UGT)	-381	-220
BGT (HL cart)	-303	-175
Permanent taxes	-59	-68
Traffic	-191	-68
Brake	-2	-1
Wind F * w	-37	-33
Temperature	-28	-1
Hot water pipe	-4	-6

Table 10 - Results of vertical load cases (in cut outside node)

Conclusion

Based on the results of the calculation with the global model, it appears that the verticals and diagonals
be critical, where the vertical of portal B is not sufficient. Using the global (bar) model for
however, the review of the portals has a number of limitations. The main limitations of the
use of the global model are:

- In the bar model, the shear force from the main beam at the top of the vertical is considered as normal force initiated and transferred as pressure to the support. In reality, the transverse force along the length of the vertical introduced by means of shear stresses. The normal force will therefore gradually increase from top to bottom.
- In the bar model it is not (properly) possible to take into account all stiffening stiffeners and with crossings of bars. For example, rigid bonds have been used over the height of the cross beam to make a connection between main beam and vertical / diagonal. in addition the stiffeners are not included in the bar model. Although the test cuts are tailored to the actual cross section of the vertical bar in the respective cut has the manner of modeling probably influences the stiffness in the model, and therefore the moment distribution the portal.
- In the bar model, the tandem systems are only entered for the design positions of the main beam. For the cross beam and for the decisive moment in the verticals the normative position should be slightly more towards the center of the crossbeam as done in the local plate model.

In consultation with Rijkswaterstaat, it has been decided to make a hybrid model for each of the portals,
consisting of a part around the portal which is completely built up with plate elements, which is coupled
is with the global bar model for the rest of the bridge. The models are described in the
Basic principles report, section 7.4.3, using the portals for the UGT assessment
made of hybrid models A, B and C. The hybrid models take into account the normative
position of the tandem system in front of the portals.

Project related

3.3.4 Portal A

3.3.4.1 Modeling

A hybrid model has been set up for portal A with a combination of bar and shell elements. The the location and dimensions of the part with scale elements have been determined in consultation with Rijkswaterstaat and has a length of approx. 10 m, from portal A to the second K-bandage, see Figure 20.

Figure 20 - The location of the part modeled with plate elements

The model is described in the basic principles report, section 7.4.3, and consists of a part that is fully modeled with plate elements (shown in red) and part that is modeled with mainly bar elements (except cover plate) (shown in pink), see Figure 21 .

Plate model

Beam model

Figure 21 - Hybrid model A consisting of a combined plate and beam model

Figure 22 - 3D view oblique-bottom view of hybrid model A.

The structure of the model and the validation of the model are discussed in the basic report and is therefore not repeated here.

Project related

3.3.4.2 Strength analysis portal A

On the basis of cross-section testing of portal A (with the global bar model) this follows in particular the vertical and diagonal are critical. Therefore, an assessment was performed with the hybrid model, based on the reduced wind load and reduced load combinations, see chapter 6.4.4 and 6.9.3.2 of the basic reporting.

To limit the calculation time of the hybrid model, only the tandem systems relevant to portal A are (position indicative for main beam and cross beam / portal) entered in the calculation model. From the analysis of the global model follows that the effect of the temperature load on the vertical of portal A is limited. In the hybrid model, therefore, the temperature loads have been neglected. The rest taxes have been retained in accordance with the global model.

From the calculation it follows that load combination 6.10b, gr1a is decisive for the vertical, with the tandem system on top of the crossbeam of the portal, the UDL load on field 1 and a wind load in x + direction (east). To get a good idea of the tensions within this combination, this is combination entered as a linear combination. This allows the actual voltage image to be viewed without an enveloping voltage picture of multiple load combinations.

In Figure 23 , the vertical stresses on one side of the slab (σ_y +) are in this normative linear ULS combination shown. Figure 24 shows the stresses in the horizontal direction of one side of the plate (σ_x +). The yield strength in the cross beam is f_y = 215 N / mm².

Figure 23 - Stresses σ $_y$ + in portal A

Figure 24 - Stresses σ $_x$ + in portal A

The stresses generally remain below the yield stress (f $_y$ = 215 N / mm²), with the exception of the stresses in the vertical at the location of the bulkhead between cross beam and cross stiffener. This is mainly caused by voltage concentrations due to the presence of welding gates and right angle connections, especially at the location of the bulkhead connection to the bottom flange of the cross beam and the connection of the bulkhead to the longitudinal stiffener.

3.3.4.3 Plastic section test vertical portal A

Because the exceedances in the vertical often occur very locally, it was examined whether the whole cross-section is sufficient on the basis of the plastic cross-section capacity. It is necessary to do this normal force and the moment in the whole section of the vertical. For this are one put four cuts in the model for which the normal force and moment occurring are determined. The cuts are taken across the flange and web of the cross stiffener plus the assisting width

of the body of the main beam. The cooperating width is limited on one side to 325 mm in connection with the end of the main beam. Therefore, a cooperating width of 2x325 = has been assumed 650 mm, see Figure 25 .

The voltages allow SCIA to integrate the voltages across the selected elements are made in the plane of the cut. This allows the normal force to be determined in the moment the relevant cut. The figure below shows the stresses in the body in the vertical direction main beam (left) and in the flange of the cross stiffener (right) shown below the standard tax combination. The cuts are shown in pink in the figures.

Project related

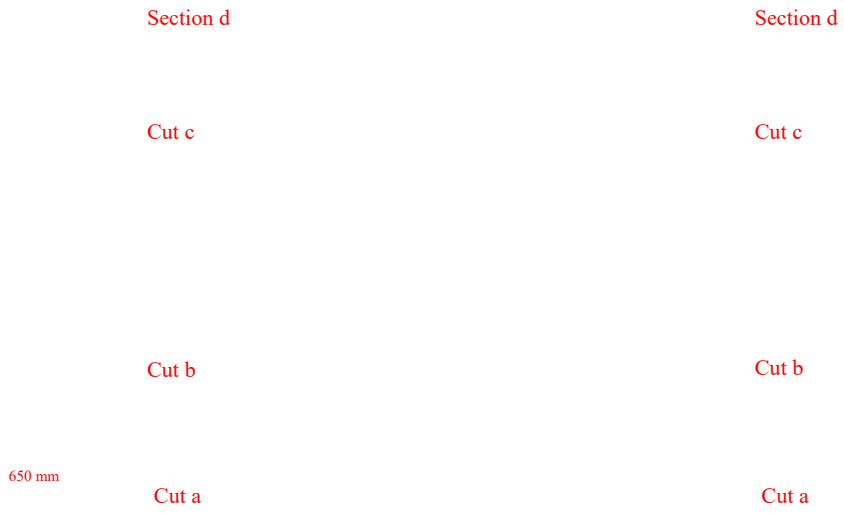

Figure 25 - Tensions σ y - in the web (left) and in the flange (right)

Based on the enveloping UGT stresses in the transverse stiffener, four critical sections have been made determined, see Figure 26 . For these cuts an integration of the forces has been performed for four

normative tax combinations. A cross-section test was then performed with this occurring forces and moments, taking into account the plastic capacity of the cross-section, see Appendix C3- q.4 to q.7.

Figure 26 - Tested cross sections in the stiffener of portal A.

Project related

The table below shows the results for the combination with reduced wind load ($c_s c_d = 0.85$) and reduced load factors.

Vertical portal A [1]

Cut	(a)		(b)		(c)		(d)	
	N_{max}	M_{max}	N_{max}	M_{max}	N_{max}	M_{max}	N_{max}	M_{max}
Occurring normal force [kN]	**-1973**	-1803	**-1427**	-1137	**-938**	-860	**-738**	-522
Normal force capacity N_{pl} [kN] -8218		-8218	**-4214**	-4214	**-3752**	-3752	**-4353**	-4353
Moment about the strong axis [kNm]	76	**94**	-4	**-12**	-39	**-62**	-59	**-122**
Moment capacity M_{pl} [kNm]	184	**184**	128	**128**	-140	**-140**	-440	**-440**
UC (strength)	**0.65**	**0.73**	**0.37**	**0.36**	**0.53**	**0.67**	**0.41**	**0.62**
UC (stability)	**0.74**	**0.82**	**0.40**	**0.39**	**0.57**	**0.73**	**0.30**	**0.40**

[1] reduced wind load ($c_s c_d = 0.85$ and $b / d_{up\ to}$ based on the width of two bridges)

Table 11 - Overview of the unity checks for testing the vertical of the K-connection at portal A (UGT)

It can be seen that, as expected, the normal force increases from top to bottom, It follows from the assessment that the vertical complies, based on the plastic capacity. The cut is just above the support (section a).

Project related

3.3.5 Portal B

3.3.5.1 Modeling

A similar hybrid model has been set up for portal B as for portal A. The location and dimensions of this part that was modeled with plate elements was determined in consultation with Rijkswaterstaat and has from 2 K-bandages before portal B to 2 K-bandages after portal B, from crossbeam with K-dressing 7 to 10, see Figure 27.

Figure 27 - The location of the part modeled with plate elements

The model is described in the basic principles report, section 7.4.3, and consists of a part that is fully modeled with plate elements (shown in red) and part that is modeled with mainly bar elements (except cover plate) (shown in pink), see Figure 28 .

Figure 28 - Hybrid model B consisting of a combined plate and beam model

Figure 29 - 3D view oblique bottom view of hybrid model B.

The structure of the model and the validation of the model are discussed in the basic report and is therefore not repeated here.

Project related

3.3.5.2 Strength analysis portal B

On the basis of cross-section tests of the portal (with the global model) this mainly follows the vertical and the diagonal is critical. Therefore, a test has been carried out with the hybrid model, based on the reduced wind load and reduced load combinations, see chapters 6.4.4 and 6.9.3.2 of the basic principles report. As for portal A, the temperature load has been neglected in the hybrid model. The other taxes have been retained in accordance with the global model.

From the calculation it follows that load combination 6.10b, gr1a is decisive for the vertical, with the tandem system on top of the crossbeam of the portal, the UDL load on fields 1, 2 and 4 and one wind load in x + direction. To get a good idea of the tensions within this combination is introduced this combination as a linear combination. This allows the weekly voltage picture to be viewed without an enveloping voltage picture of multiple load combinations.

In Figure 30 , the vertical stresses on one side of the plate (σ_y +) are in this normative linear ULS combination shown. Figure 31 shows the stresses in the horizontal direction (σ_x +).

Figure 30 - Stresses σ_y + in portal B.

Figure 31 - Stresses σ $_x$ + in portal B.

The stresses generally remain below the yield stress (f $_y$ = 215 N / mm²), with the exception of the stresses in the vertical at the location of the bulkhead between cross beam and cross stiffener, comparable as for portal A. This is mainly caused by voltage concentrations by the presence of welding gates and angled connections, especially at the location of the connection of the bulkhead on the bottom flange of the cross beam and the connection of the bulkhead to the longitudinal stiffener.

3.3.5.3 Plastic section test vertical portal B

Because the exceedances in the vertical often occur very locally, it was examined whether the whole cross-section is sufficient on the basis of the plastic cross-section capacity. Just like for portal A there are therefore several cuts have been made in the model and a plastic test has been carried out of the normative cuts. The cuts are taken across the flange and web of the cross stiffener plus the cooperative width of the main beam web ($b = 2 * 15\varepsilon t_w = 895$ mm). Supplementary to this is also made an analysis of the course of the normal force and moment in the vertical, whereby a comparison is made with the beam model.

Figure 32 - Cuts across the cross stiffener

From the voltages an integration over the selected elements can be made by SCIA in the plane of the cut. With this, a normal force line and a moment line can be composed. In the figure below shows the stresses in the vertical direction in the body of the main beam (left) and in the flange of the transverse stiffener (right) shown below the design load combination. In the on the right figure, the cuts are shown in pink.

Figure 33 - Tensions σ_y - in the web (left) and in the flange (right)

It is clear from the stress distribution in the body of the main beam that the compressive stress increases towards the support, which indicates that the normal force gradually increases over the length of the vertical, contrary to what is found in a bar model (constant normal force).

Page 41

Project related

From the integration of the stresses across the cooperative width of the main beam's body and across the transverse stiffener follows the following normal forces under the design load combination.

Figure 34 - Normal forces in the cuts

The graph below shows the normal force along the length of the vertical for two normative combinations (TS normal, normative position TS for main beam and for cross beam).

Figure 35 - Normal forces over the height of the transverse stiffener

The course of the normal force can be explained by the fact that it will build up via shear stress about the height of the main beam's body. The normal force at the bottom (-3275 kN) corresponds well with the support response for this normative combination (3216 kN) in the hybrid fashion model. In the beam model, a constant normal force over the entire height of -3096 is found kN (with the tandem system in the same position), which is therefore comparable in size. The holding of one constant normal force as found in the bar model is therefore too conservative especially for cuts at the top of the vertical.

The support reaction in the bar model comes from the main beam in field 1 for approx. 1600 kN (shear force), approx. 1150 kN from the main beam of field 2 and approx. 300 kN from the cross beam. The relatively low contribution from the cross beam is because a wheel of the axles is almost above the main beam and therefore in the

bar model will be carried over the rigid main beam.

Project related

The graph below shows that all types of loads have a comparable course in the normal force to have.

Figure 36 - Normal force per load case over the height of the transverse stiffener

If the lines were extrapolated to the top (0 m), then the normal forces due to wind and permanent loads almost back to 0 kN. The line of the traffic load decreases to approx. 300 kN, which corresponds to the wheel prints above the stand the main beam.

Page 44

Project related

The same analysis can be made for the moment line. This creates the following image found for the two normative combinations (TS normal, normative position TS for main beam and for cross beam).

Figure 37 - Moments about the height of the cross stiffener

It can be seen that the moment lines from the plate model and the beam model with the tandem system at the position which is decisive for the main beam to correspond well and thus run almost linearly over the height.
It can also be seen that when the tandem system is shifted to the normative position for the crossbeam / vertical the moments increase slightly.

Conclusion

Maintaining a constant normal force in the verticals, as found in the bar model, is too conservative. At the top, the normal forces are considerably lower than in the bar model is found. The moment line comes across well between both models, however the correct positioning of the tandem system around the find decisive moments in the portal.

Project related

Section test vertical portal B

Four critical sections have been determined on the basis of the stresses in the transverse stiffener. For this cuts, an integration of the forces has been carried out, based on 4 normative load combinations.
A cross-sectional test was then carried out with these occurring forces and moments, whereby the plastic capacity of the cross-section has been taken into account, see Appendix C3 .

Section d

Cut c

Cut b

Section d

Cut c

Cut b

Cut a

Cut a

Figure 38 - Tested sections in the cross stiffener of portal B.

The table below shows the results for the combination with reduced wind load ($c_s c_d = 0.85$) and reduced load factors.

Vertical portal B [1]

Cut	(a)		(b)		(c)		(d)	
	N_{max}	M_{max}	N_{max}	M_{max}	N_{max}	M_{max}	N_{max}	M_{max}
Occurring normal force [kN]	**-3440**	-3062	**-1463**	-1359	**-964**	-918	**-756**	-687
Capacity normal force N_{pl} [kN] -11234		-11234	**-5213**	-5213	**-4728**	-4728	**-5357**	-5357
Moment about the strong axis [kNm]	36	**90**	8	**23**	-66	**-96**	-67	**-128**
Moment capacity M_{pl} [kNm]	300	**300**	129	**129**	-116	**-116**	-310	**-310**
UC (strength)	**0.44**	**0.57**	**0.34**	**0.44**	**0.57**	**0.90**	**0.22**	**0.41**
UC (stability)	**0.48**	**0.64**	**0.37**	**0.47**	**0.57**	**0.83**	**0.36**	**0.54**

[1] reduced wind load ($c_s c_d = 0.85$ and $b / d_{up\ to}$ based on the width of two bridges)

Table 12 - Overview of the unity checks for testing the vertical of the K-connection at portal B (UGT)

It follows from the assessment that the vertical is sufficient, based on the plastic capacity. It is decisive in this the cut at the bottom of the bulkhead at the connection to the longitudinal stiffener (cut c).

Project related

3.3.6 Portal C

3.3.6.1 Modeling

A similar hybrid model has been set up for portal C as for portal A and B. The location and the
The dimensions of the part that has been modeled with plate elements have been discussed with Rijkswaterstaat determined and ranges from 1 K-bandage before portal C to 1 K-bandage after portal C, from crossbeam with K-dressing 17 to 18, see Figure 39.

Figure 39 - The location of the local model.

The model is described in the basic principles report, section 7.4.3, and consists of a part that is fully modeled with plate elements (shown in red) and part that is modeled with mainly bar elements (except cover plate) (shown in pink), see Figure 40 .

Figure 40 - Hybrid model C consisting of a combined plate and beam model

Figure 41 - 3D view oblique bottom view of hybrid model C.

The structure of the model and the validation of the model are discussed in the basic report and is therefore not repeated here.

3.3.6.2 Strength analysis portal C

On the basis of cross-section tests of the portal (with the global model) this mainly follows the vertical and the diagonal is critical. Therefore, a test has been carried out with the hybrid model, based on the reduced wind load and reduced load combinations, see chapters 6.4.4 and 6.9.3.2 of the basic principles report. As for portal A, the temperature load has been neglected in the hybrid model. The other taxes have been retained in accordance with the global model.

From the calculation it follows that load combination 6.10b, gr1a is decisive for the vertical, with the tandem system on top of the crossbeam of the portal, the UDL load on field 2, field 3 and field 5 and a wind load in x + direction (east). To get a good idea of the tensions within this combination
This combination has been introduced as a linear combination. This allows the actual voltage image without an enveloping voltage picture of several
tax combinations.

In Figure 42 , the vertical stresses on one side of the slab (σ_y +) are in this normative linear ULS combination shown. Figure 43 shows the stresses in the horizontal direction (σ_x +)

Figure 42 - Stresses σ_y + in portal C.

Figure 43 - Stresses σ $_x$ + in portal C.

The stresses generally remain below the yield stress (f $_y$ = 215 N / mm²), with the exception of the stresses in the vertical at the location of the bulkhead between cross beam and cross stiffener. This is mainly caused by voltage concentrations due to the presence of welding gates and right angle connections, especially at the location of the bulkhead connection to the bottom flange of the cross beam and the connection of the bulkhead to the longitudinal stiffener.

3.3.6.3 Plastic section test vertical portal C

Because the exceedances in the vertical often occur very locally, it was examined whether the whole cross-section is sufficient on the basis of the plastic cross-section capacity. As for portal A and B there are therefore several cuts have been made in the model and a plastic test has been carried out of the normative cuts. The cuts are taken across the flange and web of the cross stiffener plus the cooperative width of the main beam web. The cooperating width is based on the (narrowest) width of the thickening plates on the body, which extends over the entire height (w = 770 mm).

From the voltages an integration over the selected elements can be made by SCIA in the plane of the cut. This allows the normal force to be determined in the relevant cut.
The figure below shows the stresses in the vertical direction in the body of the main beam (left) and in the flange of the transverse stiffener (right) shown below the design load combination. The cuts are shown in pink.

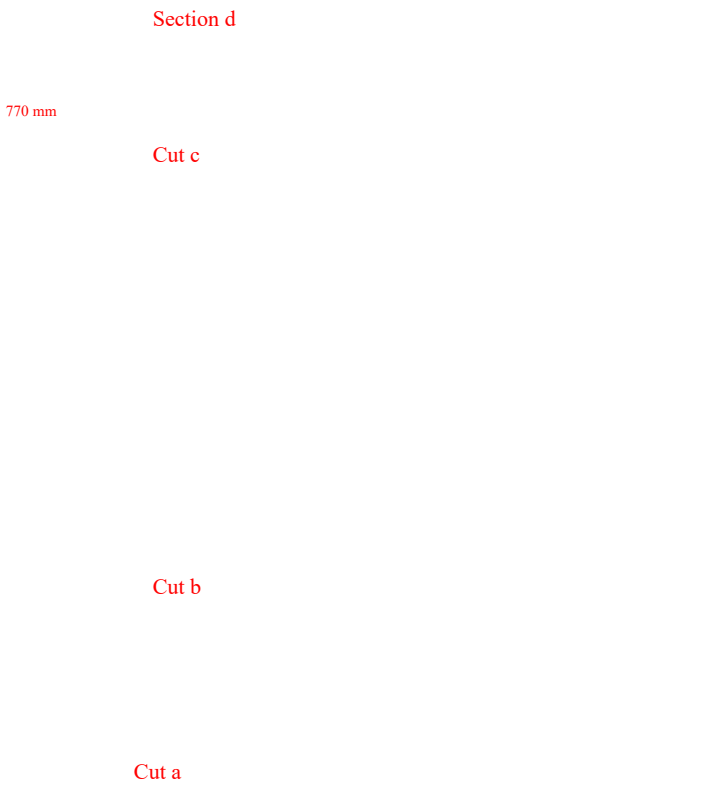

Figure 44 - Tensions σ_{y+} in the web (left) and in the flange (right)

It is clear from the stress distribution in the body of the main beam that the compressive stress increases towards the support, which indicates that the normal force gradually increases over the length of the vertical.

Cross section test vertical portal C

Four critical sections have been determined on the basis of the stresses in the transverse stiffener. For this cuts, an integration of the forces was carried out, based on the normative four tax combinations. A cross-sectional test was then carried out with these occurring forces and moments, taking into account the plastic capacity of the cross-section, see Appendix C3 .

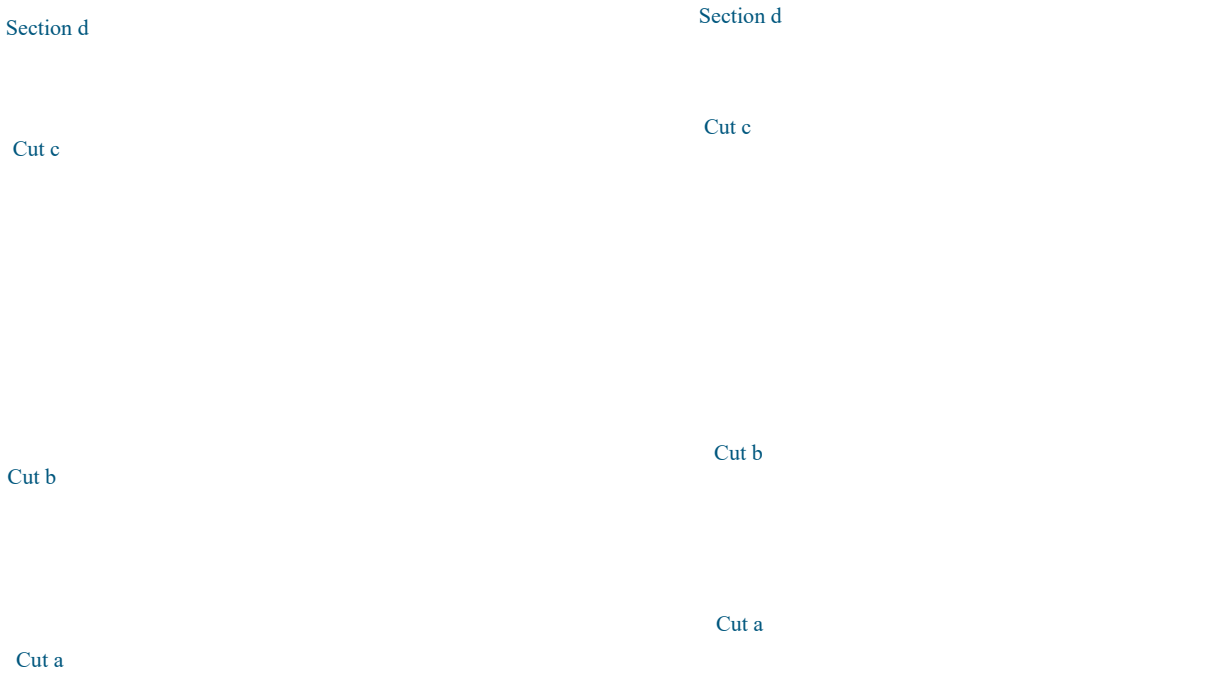

Figure 45 - Tested cross sections in the stiffener of portal C.

The table below shows the results for the combination with reduced wind load ($c_s c_d = 0.85$) and reduced load factors.

Cut	(a)		(b)		(c)		(d)	
	N_{max}	M_{max}	N_{max}	M_{max}	N_{max}	M_{max}	N_{max}	M_{max}
Occurring normal force [kN]	**-4409**	-2420	**-2442**	-2020	**-1367**	-105	**-523**	-465
Capacity normal force N_{pl} [kN]	**-13227**	-13227	**-10647**	-10647	**-9787**	-9787	**-10948**	-10948
Moment about the strong axis [kNm]	-121	**213**	-136	**-141**	-19	**-57**	-58	**-97**
Moment capacity M_{pl} [kNm]	-709	**709**	-653	**-653**	-456	**-456**	-927	**-927**
UC (strength)	**0.50**	**0.48**	**0.44**	**0.36**	**0.18**	**0.14**	**0.11**	**0.17**
UC (stability)	**0.49**	**0.40**	**0.40**	**0.39**	**0.19**	**0.13**	**0.10**	**0.11**

1 reduced wind load ($c_s c_d = 0.85$ and $b / d_{up\ to}$ based on the width of two bridges)

Table 13 - Overview of the unity checks for testing the vertical of the K-connection at portal C (UGT)

It follows from the assessment that the vertical is sufficient, based on the plastic capacity. It is decisive in this

the cut just above the support (cut a).

Project related

3.4 Steel driving deck

This chapter presents the approach and results of the testing of the steel driving deck. In front of the model output and calculations are referred to Appendix C4 .

3.4.1 Calculation approach

The steel driving deck consists of a steel plate with bulbs. Both components have been tested against it yield stress criterion. The Von Mises voltages from the local and global SCIA engineer are for this model combined.

In the local model, part of the driving deck is modeled with plate elements. This gives one realistic picture of the occurring tensions due to local effects. In the global model, the road plate is like 2D element modeled and the bulbs as 1D elements. This model has been used to estimate the global effect of normal force in the deck. All tax cases are included in both models.

The tested voltage is determined as follows:

$$_{;} = \sqrt{(+ \quad)^{2} - (+ \quad) + \quad _{2} + 3 \quad ^{2}}$$

In the global model, the road plate is based on an average normal force over half width of the riding deck. The normal forces from the rod are used for the bulbs. The figure below is see that the longitudinal stresses occur evenly across the width of the deck. Based on this, concluded that the shearlag effect is small and that it is permitted to use a average longitudinal tension over half the width of the deck.

Figure 46 - Normal voltages of the driving plate for permanent loads

The occurrence has been taken into account when adding up the stresses by the tandem system (TS) of double counting. For example, local tax effects will not necessarily coincide with global effects occur. This is particularly the case with the intermediate supports. When determining the maximum normal tensile stress above the support point is therefore considered in two load situations:

1. The maximum tensile force (from the global model) due to the load case TS occurs above the support point if the load system is in the field. This tax situation leads

however, this does not lead to additional tensions due to the local effects of the tandem system.

2. The maximum tensile stress (from the local model) occurs when the tandem system is above it support point. However, this load situation leads to low voltages due to the global effects of the tandem system.

Analysis of the results shows that the local load effects (bending in the deck) are greater than the global load effects (normal force in the deck due to bending of the main girder) and thus situation 2 is indicative of the stresses above the support point. Therefore, the normal force of it tax case TS from the global model deducted from the total enveloping ULS normal force, so that there are no load effects from two different positions of the tandem system be combined.

3.4.2 Driving board results

The normative Von Mises stresses in the road plate are presented in the table below. All parts meet the level of use. To gain more insight into the composition of the maximum voltages in Appendix C4 are the contributions of the various load components (without load factor) are summarized. The maximum von Mises stresses of the local model are from the local model together with the normative load system position shown in Figure 47 .

Location	σ_{Ed} [N / mm 2]	f_{yd} [N / mm 2]	UC
Top support (pull)	331	350	0.98
Support point bottom (pull)	273	350	0.77
Top field (pressure)	309	350	0.92
Bottom side (pressure)	292	350	0.84

Table 14 - Overview of unity checks driving plate

Figure 47 - Maximum Von Mises voltages (local model) with location-determining load system

Project related

3.4.3 Bulb results

The maximum tensile and compressive stresses of three locations have been determined for the bulbs; the consoles (bulb 2), near the main beam (bulb 7) and in the middle of the driving deck (bulb 14). In the table below are the Von Mises tensions determined. The global and local tax effects have also been added for the bulbs corrected for double counting from the tandem system.

Figure 48 - Locations of the bulbs

The maximum UC occurs at the point of support of bulb 2. However, the exceedance is very high minimal. When calculating with the reduced wind load and reduced tax combinations, as described in the basic report (sections 6.4 and 6.9), the unity checks fall below 1.0.

Part	Location	σ_{Ed} [N / mm 2]	f_{yd} [N / mm 2]	UC

Bulb 2	Support point (pull)	365	350	1.04
	Field (pressure)	268		0.77
Bulb 7	Support point (pull)	352	350	1.01
	Field (pressure)	239		0.68
Bulb 14	Support point (pull)	349	350	1.00
	Field (pressure)	207		0.59

Table 15 - Overview of unity checks bulbs

Page 54

Project related

3.5 Bearings and jacking points

3.5.1 Vertical support reactions

Support reactions have been compared to design loads. According to drawing [A.21582] and [A.21583] the design capabilities are as follows.

					south
Pillar F	Pillar G	Pillar H	Pillar J	Pillar K.	LH

Figure 49 - Design values for capacity of supports

At the site of Pillar J, a new spherical segment for the eastern bridge is being laid.
It has a vertical capacity of 8511 kN (UGT) according to [17245-ONT-001_02]. In the western
the current role imposition remains.

When the bridge was built, it was customary to test the capacity against the BGT value
of the occurring taxes. The capacity took into account a safety factor of
normally 1.5. Therefore, for the comparison, the design loads have been multiplied by a factor
1.5 to arrive at a UGT capacity. The following support reactions are used in the Scia calculation
found in the UGT. It is noted that the bridge in the model is half loaded with tandem systems
plus a tandem system at pillar J. The highest reaction forces of pillar F and G therefore serve
be maintained symmetrically for the unloaded side.

Project related

The following support reactions are found in the calculation.

Figure 50 - UGT support reactions

Based on these support reactions and design capacities, the table below shows the comparison summarized.

Fulcrum	Rz [kN]	Design load (BGT) [kN]	Capacity (BGT x 1.5) [kN]	UC
Pillar F	2275	1580	2370	0.96
Pillar G (pressure)	3813	2030	3045	1.25
Pillar G (pull)	529	360	540	0.98
Pillar H (fixed solution)	8702	5920	8880	0.98
Pillar J (roll up)	8646	5920	8880	0.97
Pillar J (bolsegm.)	8646		8511	1.02

Table 16 - Comparison support reactions ULS with design values

The support reaction at pillar G is greater than the design value according to the drawing. The support response ter location of pillar J is greater than the design value according to the calculation in [17245-ONT-001_02]. There is therefore looked at the support response under the reduced wind load and reduced tax combinations, as described in the basic report (sections 6.4 and 6.9). With this the support reaction on pillar J is sufficient, but it is not yet sufficient on G.

Fulcrum	Rz [kN]	Design load (BGT) [kN]	Capacity (BGT x 1.5) [kN]	UC
Pillar G (pressure)	3550	2030	3045	1.17
Pillar J (bolsegm.)	8281		8511	0.97

Table 17 - Comparison of support reactions ULS with reduced load combinations with design values

Project related

For the roll bearing at pillar G, therefore, a little more attention has been paid to the possible reserve that is still in stock the calculation is done. In the NET calculation, a (re) calculation of the imposition has been carried out. Herein was Assumes a support response of 182.17 tons, whereby the benchmark test is the assessment of the bottom plate is with a UC of 2164/2400 = 0.90, When it is recalculated to a UC of 1.0, a maximum (BGT) capacity of 182.17 / 0.90 = 202 tons is found. This is almost equal to the capacity according to drawing (203 tons). On the basis of this it could therefore be concluded that there are no spare capacity in the support is in relation to the capacity in the drawing.

Figure 51 - Excerpt from [BBV-0010-01]

However, in this calculation it is assumed as a conservative starting point that the bottom plate in the clamped in the middle, assuming the projection in the longitudinal direction of the roll. In reality will however, the load transfers its load in the width direction and can therefore be of a considerably wider nature distribution are assumed than the 2 cm used. This tension will therefore never be decisive to be.

The next decisive part of the connection is the role. For this a capacity of 219.84 tons were found, which corresponds to a UGT capacity of 3298 kN. From the SCIA calculation follows a support reaction of 3550 kN among the (reduced) ULS combinations, with a UC = 1.08 is found.

Figure 52 - Excerpt from [BBV-0010-01]

When this assessment is carried out in accordance with the current standard (NEN 1337-4: 2005), a characteristic resistance of the contact pressure per unit length found from:

$$' = 23 * * = 23 * 200 * \frac{600^2}{210000} = 7.89 /$$

Assuming a length of 458 mm and $\gamma_m = 1$, a capacity of

$$' = {}_2 * 458 = 7.89 * 458 = 3612$$

Assuming a support reaction under the (reduced) ULS combination, a UC = 0.98 found, which satisfies the imposition.

Project related

3.5.2 Horizontal support reactions transverse direction

No design capacities of the supports are known. Therefore, the capacity is determined analogously to the (re) calculation [BBV0010-01]. According to SCIA, the horizontal support reactions below are found it. For Pillar J these are given in the bearing point halfway down the lower edge, for the new one situation in the eastern bridge. For the western bridge, this support reaction is split between the two roller bearings and are therefore comparable to pillar H.

Figure 53 - Horizontal support reactions in the transverse direction of UGT (western main beam + center support pillar J)

Figure 54 - Horizontal support reactions in transverse direction UGT (eastern main beam)

Pillar F and G

The capacity is determined analogous to the recalculation [BBV-0010-01]. It is decisive pressure surface (cam) on the top and bottom of the roll. In the recalculation [BBV-0010-01] is erroneous assumes a capacity of 2x tensile strength. This appears to be an error and has therefore not been applied.

Figure 55 - Fragment of calculation of ridge supports 158 tons and 203 tons from [BBV-0010-01]

Based on the new taxes, the following calculation can be made analogously.

Pillar F / L

F_h = 176 kN (ULS)

$\sigma_{vl.dr}$ = 176 kN / 12.9 cm² = 136 N / mm²

$f_{vl.dr}$ = 340 N / mm²
UC = 136/340 = 0.40

$\tau_{f,Ed}$ = 176 kN / (15.4 cm x 3.8 cm) = 30 N / mm²
$\tau_{f.Rd}$ = 0.58 * 340 N / mm² = 197 N / mm²
UC = 30/197 = 0.15

Pillar G / K

F_h = 437 kN (ULS)

$\sigma_{vl.dr}$ = 437 kN / 12.9 cm² = 338 N / mm²

$f_{vl.dr}$ = 340 N / mm²
UC = 338/340 = 1.00

$\tau_{f,Ed}$ = 437 kN / (15.4 cm x 3.8 cm) = 75 N / mm²
$\tau_{f.Rd}$ = 0.58 * 340 N / mm² = 197 N / mm²
UC = 73/197 = 0.38

Pillar H (fixed support)

No horizontal capacities are given for pillar H. Also in the recalculation there is no further
calculated on the basis of the horizontal capacity of the fixed support points. Therefore, no statement can be made about this
whether it is satisfactory. It is recommended to recalculate this.

Pillar J (roll bearing)

The ridge of the existing roller support at pillar J is slightly larger. In addition, there are two roles
present, making the surface twice as large.

Figure 56 - Fragment of calculation cam roller bearing 592 tons from [BBV-0010-01]

Based on the new taxes, the following calculation can be made analogously.

Pillar J (roll bearing)

F_{h} = 1892 kN / 2 = 946 kN (ULS)

$\sigma_{vl,dr}$ = 946 kN / 2x15.8 cm² = 299 N / mm²

$f_{vl,dr}$ = 340 N / mm²
UC = 299/340 = 0.88

$\tau_{f,Ed}$ = 946 kN / 2x16.2 cm x 3.8 cm = 77 N / mm²
$\tau_{f,Rd}$ = 0.58 * 340 N / mm² = 197 N / mm²

UC = 77/197 = 0.39

Pillar J (transverse fixation lower edge of portal)
At the location of the eastern bridge, next to the spherical segment bearings (rolling in both directions), a horizontal fixation point placed halfway down the bottom edge of the portal. Conforms [17245-ONT-003] this fixation point is designed for a horizontal support reaction of 1650 kN. The occurring horizontal support reaction is 1892 kN. The imposition would not suffice with this. However, when calculating with a reduced wind load with cscd = 0.85 and b / d based on 2 bridges, an approx. 30% lower wind load, and therefore support reaction was found. The horizontal support reaction with this adjusted wind load is 1342 kN, whereby a UC = 1342 kN / 1650 kN = 0.81 is found.

Pillar J (transverse fixation lower edge of portal)

Fulcrum	UC pressure	UC shear
Pillar F / L	0.40	0.15
Pillar G / K	1.00	0.38
Pillar H (fixed support)		
Pillar J (roll bearing)	0.88	0.39
Pillar J (transverse fixation)	0.81	n / a

Table 18 - UC's Impositions

3.5.3 Horizontal support reactions in the longitudinal direction

In pillar H, in addition to the support reactions in the transverse direction, support reactions in the longitudinal direction also occur. The figure below shows the support reactions found. The same applies to the longitudinal direction horizontal capacities of the support are given in the design and recalculations. You can do this therefore no statement is made as to whether it is sufficient. It is recommended to recalculate this to feed. It is noted, however, that the horizontal support reactions in the longitudinal direction are relatively high and in are largely caused by the fully fixed modeled supports. In fact the bearings have spelling, so that the winding forces will be lower.

Figure 57 - Horizontal support reactions in the longitudinal direction UGT

3.5.4 Support reactions per tax case

To gain more insight into the tax payments of the various tax cases, see
the table below shows the contributions of the various tax components (without tax factor)
summarized.

		Pillar F			Pillar G				Pillar H		
		$R_{X,max}$	$R_{Y,max}$	$R_{Z,max}$	$R_{X,max}$	$R_{Y,max}$	$R_{Z,max}$ [1]		$R_{X,max}$	$R_{Y,max}$	$R_{Z,max}$
UGT	[kN]	0	176	2275	0	437	3813	-529 3983		940	8702
BGT	[kN]	0	126	1833	0	306	3046	-142 2971		637	6898
Permanent	[kN]	0	2	535	0	7	801	771	22	14	2634
Traffic	[kN]	0	37	1101	0	75	1834	-587 1477		37	2723
Brakes	[kN]	0	2	4	0	0	30	-30	351	0	19
Wind F * w	[kN]	0	74	138	0	218	328	-328 1059		582	1331
Temperature	[kN]	0	42	49	0	36	26	-26	57	42	27
Hot water pipe [kN]		0	0	41	0	0	53	0	115	1	187

1 negative values are tensile forces

Table 19 - Results of load cases for reaction forces

3.5.5 Auger points

The jacking points are tested against the bearing stress at the location of the body, in the cut just above the bottom flange of the main beam. In addition, part of the tax will be paid through the body upwards and thereby cause a transverse load in the plate field. This transverse load should be tested for interaction with the longitudinal stresses and is therefore included in the pleat checks of sections G-1 and H-1, see Appendix C1. b and c.

Imposition tension body and stiffener

In the cut just above the body, a test was performed on the comparison voltage, based on a spread of the support pressure at 45 ° in the bottom flange. Stiffeners are fitted on both sides of the body, which are included in the surface. The bridge is assumed to be fully loaded during the jacks and that each jack point absorbs 50% of the load (hydraulically coupled jacks).

Figure 58 - Mounting surfaces of jacking points at pillar G (left) and pillar H (right)

The results are summarized in the table below. For the body, the longitudinal stresses.

Fulcrum	$\sigma_{cf.,Ed}$ [N / mm 2]	f_{yd} [N / mm 2]	UC
Pillar G (body)	262	350	0.75
Pillar G (stiffener)	85	215	0.48
Pillar H (body)	307	350	0.88
Pillar H (stiffener)	156	215	0.73

Table 20 - Overview of unity checks imposed pressure above jacking points

Cross-sectional load assessment

It is assumed that the transverse load above the jacking points is partly through the thickening plates transferred to the cross stiffeners above the normal support point. The other part is through the web plate paid yourself. For the distribution of taxes between these two systems it is assumed that these are divided on the basis of the thickness of the different plates. The tensile strengths are tested pressure diagonals in the thickening plates and the interaction between fold and transverse loads in the body above the jacking points, see Appendix C1 .b and c. In the figures below, the sustained pull (red) and pressure (blue) diagonals, including the adhered widths.

Figure 59 - Payment of the transverse loads in the thickening plates at pillar G (left) and pillar H (right)

Fulcrum	$\sigma_{cf.,Ed}$ [N / mm 2]	f_{yd} [N / mm 2]	UC
Pillar G (pressure diagonal)	175	215	0.81
Pillar G (drawstring)	210	215	0.98
Pillar G (transverse load η_2)	UC = $\eta_2 = F_{vp} / F_{Rd}$		0.42

Pillar G (pleat interaction and transverse	UC = (η_1 + 0.8 * η_2) / 1.4		0.75
Pillar H (printing diagonal)	161	215	0.75
Pillar H (drawstring)	192	215	0.89
Pillar H (transverse load η_2)	UC = η_2 = F_{vp} / F_{Rd}		0.60
Pillar H (pleat interaction and transverse	UC = (η_1 + 0.8 * η_2) / 1.4		1.01

Table 21 - Overview of unity checks imposed pressure above jacking points

NB. The above calculation is conservative, because the calculation assumes that it first field can also fold. In reality this is not the case, because here a body three times as thick is present with a shot on both sides.

Project related

In the document “commentary to EN 1993-1-5”, a number of changes are proposed in chapter 6.4. A clearer distinction is also made here between the fold of the first field and the fold of the body all over the height. A calculation has therefore also been made with these modified formulas. This finds slightly more favorable UCs.

Fulcrum	$\sigma_{cf.,Ed}$ [N / mm 2]	f_{yd} [N / mm 2]	UC
Pillar G (transverse load η_2)	UC = η_2 = F_{vp} / F_{Rd}		0.38
Pillar G (pleat interaction and transverse	UC = (η_1 + 0.8 * η_2) / 1.4		0.73
Pillar H (transverse load η_2)	UC = η_2 = F_{vp} / F_{Rd}		0.52
Pillar H (pleat interaction and transverse	UC = (η_1 + 0.8 * η_2) / 1.4		0.96

Table 22 - Overview unity checks transverse loads above jacking points in accordance with “commentary to EN 1993-1-5”

It has been demonstrated that the jacking points are sufficient.

3.6 Inspection path

In this chapter the results of the inspection path inspection are presented. For the

calculations are referred to Appendix C5.

3.6.1 Calculation approach

A distinction is made in the calculations between the normal consoles and the “reinforced” consoles have a light pole at the end. The moments in the consoles are determined using a hand calculation in Mathcad. For the consoles with a light tower, wind has been taken into account bend if torsion in the console.

3.6.2 Results of inspection path

All consoles of the inspection paths comply with strength and stability. The reinforced console is no further tested for stability (tipping) due to the low UC on strength.

Profile diagonals	get well soon	stability
Normal console	0.75	0.95
Reinforced console with light pole	0.14	

Table 23 - Unity checks Inspection path

Project related

4 Connections

4.1 Connection type A - Weld connection on bottom plate flange main beam

In the lower flange are at a number of places a 2 e flange plate disposed below the lower flange. To the end of this outer flange plate, the tension in the plate must be welded to the 1 st flange plate are transferred. At the end of the flange plate, a bevel is provided in both the width as the thickness (from 30 mm to 10 mm).

Figure 60 - Detail type A4 (left) and A5 (right)

The design end is based on the stresses in the lower flange in the cut with an extra covering plate determined. Connection A1, A4 and A5 were tested. Connection A2 and A3 have a lower voltage as A1 and A4 respectively.

The welds were tested using Mathcad, see Appendix D1 . This is based on the force in the 2 nd cover plate, which is transferred to the bottom flange via the weld. For the length of the weld starting from the end part (L1), the inclined part (L2) and if necessary part of the weld that runs parallel to the bottom flange (L3). Initially it was tested whether the weld is satisfactory if only L1 and L2 be included (UC_{las1+2}). If this is not sufficient, the length of L3 the weld connection satisfactory ($UC_{weld1+2+3}$). The result of the calculation is summarized in Table 24 . Because the in principle, a longer part of the weld may also be taken along, which the UC uses reality is lower than what is indicated in Table 24 .

Detail Type A: Weld against end of thickening plate

Code	Cross beam number	Additional description	dx	σ below, max	σ below, min	L1 [mm]	L2 [mm]	L3 [mm]	$UC_{weld1+2}$	$UC_{weld1+2+3}$
A1	6-7	Thickening plate end 350 mm wide	10000	191	10	70	424	400	1.71	<0.90
A2	19-20	Thickening plate end 350 mm wide	33498	174	-27	70	424	400	<1.7	<0.90
A3	39-40	Thickening plate end 550 mm wide	68962	81	-163	70	599	1000	<2.57	<0.98
A4	57-58	Thickening plate end 550 mm wide	100953	-5	-254	70	599	1000	2.57	<0.98
A5	74-75	Thickening end 530 mm wide	124584	197	-21	0	954	0	0.43	<0.43

Table 24 - Stresses in bottom flange and Unity check of the welded joint at the end of the screed plate

The relative low UC of Compound A5 can be explained in that the second e opdikplaat only 10 mm thick, , so that the force that must pass through the weld is relatively small compared to connection A1 to A4 (t = 30 mm).

Project related

4.2 Connection type B and C - Riveted connections bridge sections

The bridge was supplied in bridge sections during construction and then riveted together. On the spot of these section divisions, various coupling plates in the bottom and top flange and the body have been used every connect section parts together. This section describes the rivets and connecting plates tested from the main beam.

Figure 61 - Detail type C - riveted section division connection (shown is connection C1)

Project related

Initially, based on the stresses in the main beam, cuts are made at the
the divisional connections determined in section divisions. Connection C1 and C8, the two, have been tested
joints with the highest tensile stress in the bottom flange. The voltages shown are determined as
the stresses without the flange extenders. The actual voltages will therefore be slightly lower.

Detail Type C: Riveted connection bridge sections	M_{max}	M_{min}
	Ash	
Cross beam		

Code	number	Additional description	section-division	dx	σ above	σ below	σ above	σ below
C1	11-12	Riveting in section division in field 1	2	18499	-141	**252**	0	7
C2	21-22	Riveting in section division in field 1	4	36897	-82	195	22	-62
C3	28-29	Riveting in section division in field 2	5	49095	-35	68	61	-155
C4	36-37	Riveting in section division in field 2	7	63783	-68	158	80	-225
C5	46-47	Riveting in section division in field 2	9	81631	-24	24	135	-222
C6	60-61	Riveting in section division in field 3	12	106764	-9	17	103	-260
C7	69-70	Riveting in section division in field 3	14	122510	-90	213	15	-38
C8	79-80	Riveting in section division in field 3	139630	16 -195		**315**	11	21

Table 25 - Stresses in the main beam at the section divisions

The connections have been tested using Mathcad, see Appendix D2. The rivets and the net cross sections of the main beam and the coupling plates. The result of the calculation is summarized in Table 26.

Detail Type C: Riveted connection bridge sections	Connection C1				Compound C8	
Test aspect	Top flange	Body	Lower flange	Upper flange	Body	Bottom flange
Shear rivets	0.39	0.62	0.70	0.48	0.88	0.85
Net cross section of main beam	0.41	0.73	0.74	0.56	1.00	0.98
Net cross section connecting plates	0.28	0.46	0.62	0.38	0.62	0.81

Table 26 - Unity checks connection C1 and C8

It follows from the assessments that the net cross-section in all parts is decisive. The tensile stresses in the the main beam at the location of the other sections is lower, so it can be assumed that the other connections will also suffice. The compressive stress in connection C6 is (slightly) higher than in connection C8, but in view of the low UC's of the top flange and the fact that pressure may be used of the gross cross-section, it can be assumed that this connection will more than meet the strength requirement.

4.3 Connection type K - Rivet connection flange package

Rivets are used in the bottom flange of the main beam to hold the plate pack together.
At the cut with the highest tensile stress (center field 3) is a test on the net
done section.

Figure 62 - Detail type K - Rivet connection flange package

A unity check of 1.04 is found in the net cross section of the lower flange . Hereby is
take into account reduced cross-section due to pleat. That is why we also looked at the tension
under the reduced load combinations, as described in sections 6.4 and 6.9 in the
principles report. Under this combination, a UC of 0.97 is found, which means
it is concluded that the connection will then suffice.

4.4 Connection Type L - Connection console / cross beam with main beam

4.4.1 Connection L1 - Connection console - main beam

The console is connected to the body of the body by means of angle brackets on the body and under the lower flange main beam. A widened plate is provided in the bottom flange. The top flange of the console is coupled at the top with the cross beam and the top flange of the main beam.

Figure 63 - Detail Type DD-zK1 Console - main beam connection (left side view, right widened plate and angle steel bottom flange)

The connection has been tested on the basis of the cutting forces determined in the local model of the deck construction. For this, the stresses in the bottom flange, web plate and deck are integrated into one normal force, transverse forces and moments at the area of the cut at the joint, see Appendix D4a . A width of 300 mm is used for the deck, corresponding to the width of the connecting plate of the top flange. The cutting forces were then translated into forces in the connecting means (rivets, angle bars and plates) in the connection. It is hereby assumed that the rivets in the body do not contribute to the transfer of the moment, because they will be less rigid react by connecting with angle brackets. The various components have been tested using Mathcad, see Appendix D4b .

Detail Type DD-zK1: Console - main beam connection

Part	Rivets	Net cross-section console	Net cross-section link
Top flange	0.52	0.39	0.39
Body	0.22	0.40	0.31
Console bottom flange - bottom flange plate	0.58	0.39	0.43
Bottom flange plate - angle steel	0.87	0.39	0.25

Table 27 - Unity checks connection L1 console - main beam

4.4.2 Connection L2 - Cross beam - main beam connection

The cross beam is connected to the main beam in a similar way to the console. Divergent for the connection of the cross beam to the connection of the console is welded headboard and the welded connection of the bottom flange.

Figure 64 - Detail Type DD-zK2 Cross beam - main beam connection (left side view, right side head plate view)

The connection has been tested, based on the connection of the console, on the basis of the cutting forces determined with in the local model of the deck construction. For this are the tensions in the lower flange, body (including knee bulkhead) and deck, integrated to a normal force, transverse loads and moments at the location of the cut at the joint, see Appendix D4c . Thereby both a cutting forces determined at the connection of an intermediate cross member as at a cross member with K-bandage. The cutting forces were then translated into forces in the connecting means (rivets and welds) in the joint. These parts have been tested using Mathcad, see Appendix D4d . The results of the calculations are summarized in the table below.

Detail Type DD-zK2: Cross beam - main beam connection

Part	Rivets	Net cross-section console	Net cross-section link	Weld connection
Top flange	0.46	0.34	0.34	
Body	0.23			0.26
Bottom flange				0.70

Table 28 - Unity checks connection L2 crossbeam - main beam

Project related

4.5 Connection type P - Diagonals K-connections and portals

At the top of the diagonals there is a rivet connection to the top
knee shot under the cross bar and at the bottom with the bottom edge. The connections at the top
and bottom are almost identical, so the benchmark of the four has been tested.

Figure 65 - Type P connection Diagonals K-braces - main beam

The cutting forces at the end of the bar are translated into forces in the connecting means
(rivets) in the joint. The rivets and the net diameter of the diagonals and
connecting plates have been tested using Mathcad, see Appendix D5 . For the connection of portal C.
it was necessary to maintain a plastic distribution of the moments and normal forces. The
results of the calculations are summarized in the table below. In the first instance, the
connections of portal B and C are not. That is why it was examined whether the connections are sufficient for a
reduced wind load, as described in the strength test of the portal (section 3.3.3) . Bee
this reduced wind load meets all connections.

Detail Type P: Connection diagonals K-connections and portals

Part	Rivets	Net cross-section profile	Net cross section plate
K bandage 2xL80x80x8	0.08	0.34	0.26
K-bandage 2xL90x90x9	0.12	0.40	0.41

Portal A	0.32	0.66	0.83
Portal B	1.18 / 0.94 1	1.06 / 0.92 1	0.80 / 0.70 1
Portal C	1.16 / 0.84 1	1.30 / 0.95 1	1.30 / 0.95 1

1 reduced wind load (CsCd = 0.85 and B / D based on the width of two bridges

Table 29 - Unity checks connection type P - diagonals K-connections and portals

Project related

To gain more insight into the shares of taxes to the forces in the compound are in the table below shows the contributions of the various tax components (without tax factor) summarized in the cut with the maximum UC. The UC is determined by both N and My.

tax	Portal B		Portal C	
	N [kN]	M_y [kNm]	N [kN]	M_y [kNm]
UGT	-537	-4.3	-1611	-67.6
BGT	-390	-3.5	-1082	-47.3
Permanent taxes	-44	-1.0	-32	-8.7
Traffic	-116	-2.0	-64	-1.7
Brake	-2	-0.0	0	-0.1
Wind F * $_w$	-214	-0.3	-1038	-35.1
Temperature	-36	-0.0	-11	-0.8
Hot water pipe	-3	-0.1	-1	-0.4

Table 30 - Normal force and moment contributions (N + My) of the different load components in connection P.

It can be seen that in portal B traffic in particular makes a major contribution to the moment in the connection, while Wind F * $_{w\ makes}$ a big contribution to the normal force. For Portal C, Wind F * $_w$ is responsible for almost the full normal force and most of the moment.

Project related

4.6 Connection type Q - Bottom and top edge K-bandages and portals

The bottom and top edges of the K-bandages and the portals are connected to the cross stiffeners on the body of the main beam.

Figure 66 - Detail type Q - Connection bottom edge K-bandages - main beam (left) and bottom edge portal C (right)

The cutting forces of the bottom and top edges are translated at the center of the joint to forces in the connectors (rivets). The rivets and the net diameter of the bottom and top edge and the connection plates are tested using Mathcad, see Appendix D6 . The results of the calculations are summarized in the table below.

Detail Type Q: Connection bottom and top edge K-bandages and portals

Part	Rivets profile	Rivets at stiffener	Net intersection profile	Net intersection plate	Head plate and shot up top flange

Bottom edge of portal A	0.39	0.46	0.39	0.31	
Top edge of portal A	0.83		0.33	0.53	
Bottom edge of portal B	0.63		0.12	0.24	0.88
Lower edge of portal C (at the spherical segmentation)	1.47 / 1.16 1		0.91 / 0.72 1	0.78 / 0.62 1	
Lower edge of portal C (at fixed support and existing role imposition)	2.49 / 1.85 1		1.35 / 1.00 1	1.45 / 1.07 1	
Top edge of portal C	0.34		0.42	0.48	

1 reduced wind load (CsCd = 0.85 and b / d up to based on the width of two bridges) and load combinations

Table 31 - Unity checks connection Q - bottom and top edge K-connections and portals

Project related

For portal C, a distinction has been made between the existing fixed supports (pillar H, both) bridges) and the existing roller bearings (pillar J, western bridge) and the (new) spherical segment support, with a horizontal support halfway down the lower edge, (pillar J, eastern bridge). A lower UC is found for the connections of portal C at the location of this last pillar, because the force is transferred from the diagonals directly to the horizontal support and not need to go through the connection. It is noted that in the SCIA calculation a higher moment is found in the connection of the lower edge of portal C at the spherical segment support as in the draft note from edilon sedra [17245-ONT-003]. The difference with this calculation is in the size of the horizontal support reaction.

Only the connections of the lower edge of portal C are initially unsatisfactory. The calculation of the connections at portal C have therefore been repeated with the model in which the wind load is is reduced on the basis of c s c d = 0.85, and b / d to ratio of the two bridges, in combination with the reduced tax combinations in accordance with sections 6.4 and 6.9 of the basic principles report. In front of the explanation is referred to section 3.3. 3. Also comply with this reduced load the connections at portal C are not. These will therefore have to be strengthened.

The contributions are shown in the table below to gain more insight into the cause of the exceedances of the different load components (without load factor) summarized for the cut in the bottom edge of portal C at the junction, based on the model without reduction of the wind load. The UC is mainly determined by the moment M y at the location of the connection. To you can see that the wind load makes the biggest contribution.

tax	Moment M y (Sliding bearing) [kNm]	Moment M y (Fixed imposition) [kNm]

UGT	-107	-151
BGT	-78	-107
Permanent taxes	-14	-16
Traffic	-16	-14
Brake	0	0
Wind F * w	-44	-75
Temperature	-6	-3
Hot water pipe	-1	-1

Table 32 - Moment contributions (My) of the various tax components in compound Q.

Project related

4.7 Connection type R - Rivet connection at section divisions

At the section divisions, rivet connections have been used in the deck and the bulbs. The deck is connected to a plate on the top and bottom of the deck and the bulbs with a plate on on both sides of the body. To be able to apply the plate to the underside of the deck is part of the body of the bulbs, removed just below the deck, after which a plate is welded underneath.

Figure 67 - Detail type R - Connection of deck construction (top) and bulbs (right)

The connection in the deck has been tested at the section division where the greatest stresses occur from the global behavior. The table below shows the tensile and compressive stresses in the top flange of the

main beam again at the site of the section divisions. The largest tensile stress is found on axis 5, op shaft 8 the greatest compressive stress. Therefore, for these cuts, the connection was checked, where the stresses from the local model (deck construction) have been taken into account.

Detail Type R: Riveted connection bridge sections

Code	Cross beam number	Additional description	Ash section-division	dx	σ min	σ max
R1	11-12	Riveting in section division in field 1	2	18499 -141		0
R2	21-22	Riveting in section division in field 1	4	36897-82		22
R3	28-29	Riveting in section division in field 2	5	49095 -35		61
R4	36-37	Riveting in section division in field 2	7	63783 -68		80
R5	46-47	Riveting in section division in field 2	9	81631 -24		**135**
R6	60-61	Riveting in section division in field 3	12 106 764-9			103
R7	69-70	Riveting in section division in field 3	14 122 510 -90			15
R8	79-80	Riveting in section division in field 3	139630 16 **-195**			11

Table 33 - Stresses in the top flange of the main beam at the section divisions

Project related

The rivets and the net cross section of the deck construction (bulb, deck plate) and the connecting plates are tested using Mathcad, see Appendix D4g . The results of strength testing are summarized in the following table.

Detail Type R: Rivet connection deck construction at section divisions

Part	Rivets	Net intersection deck / bulb	Net cross-section connecting plate
Connection cover plate at section division R5	0.60	0.65	0.38
Connection bulbs at section division R5	0.65	1.01 / 0.99 1	0.86
Connection cover plate at section division R8	0.96	0.85	0.56
		0.67	

Connection bulbs at section division R8	0.54	0.57

1 reduced wind load and load combination cf. basic report §6.4 and §6.9

Table 34 - Unity checks connection R - cover plate and bulbs

The connection of the bulbs is just not sufficient in the assessment of the net cross-section of the deck construction. However, the calculation does not conservatively take into account the fact that a (small) part of the voltage is already through the weld between the body bulb and the connecting plate at the bottom of the deck transferred in the part for the first rivet row. When this is included, the construction will comply. The construction is also satisfactory when calculating with the reduced tax combination.

Project related

4.8 Connection type S - Long stiffeners

In the main bridge, the sections of the main beams are designed as a rivet connection. Ter
At the location of these section divisions, the longitudinal stiffeners are coupled with riveted corner profiles, see Figure 68.

Figure 68 - Detail type S - Connection between the longitudinal stiffeners at section divisions

In Appendix D8 , the stresses in the longitudinal stiffeners for each section division are determined on the basis of the UGT tax combinations and the individual tax components. Although the tensions in the longitudinal stiffeners themselves at the location of the section division are lower than the yield stress, it appears that due to the eccentric connection of the coupling creates additional moments that cause it connecting piece and the longitudinal stiffener can flow. If it is assumed that the moment completely absorbed by the coupling piece and the longitudinal stiffener, very great stresses are created the UGT. However, it is likely that some of the bending is caused by the main beam's web plate will be included. To properly calculate the distribution of the stresses in the To determine the longitudinal stiffener, the coupling piece and the body plate, a plate model of the connection has been made using DIANA. Besides determining the voltage distribution, the aim of this model is also the determining the deflection of the web plate and the longitudinal stiffener by flowing (parts of) the link. Namely, a large deflection can lead to a reduced support against bending stability.

A detailed explanation of the model and modeling is provided in Appendix D8. Figure 69 shows it DIANA model where the edges of the model match the connection of the body to the bottom flange (bottom), the second longitudinal stiffener (top) and the cross stiffeners (left and right) of the field with the link. Plate elements and contact elements have been used for the model. To the plate elements are assigned non-linear material properties, so that the flow can be included turn into. On the right side of the model there is one on the plate edge and the edge of the longitudinal stiffener tension of 170 N / mm² applied, corresponding to the maximum tension in the ULS.

Contact element between
longitudinal stiffener and gusset plate

Contact element between
longitudinal stiffener and connecting piece

Figure 69 - FEM model with coupling piece and contact elements.

The model has been calculated linearly and non-linearly. The following follows from the non-linear calculation voltage picture.

Figure 70 - Von Misses stresses non-linear calculation in the fully loaded situation (170 N / mm²) (front view).

Figure 71 - Von Misses stresses non-linear calculation in the fully loaded situation (170 N / mm²) (top view).

It can be seen that flow of the connection occurs in the coupling piece. None occur in the longitudinal stiffener itself flow up.

In addition to the analysis of the stresses, the deformations from the plane of the body were also examined. This one deformations can theoretically affect the main beam's bending stability.

Figure 72 - Distortion from the plane of the web according to the non-linear analysis for the UGT load (170 N / mm²).

The maximum deformation of the web plate itself is 0.09 mm in the non-linear calculation. This maximum deformation occurs at the connection with the longitudinal stiffener.

When these deformations are compared with the allowable eccentricities according to the Eurocode, it can be concluded that this extra distortion is negligibly small. So it becomes according to NEN-EN 1993-1-5 table C.2 assumed a longitudinal stiffener with length a and beam height b from the minimum of a / 400 and b / 400. This amounts to 1800/400 = 4.5 mm. It is concluded that the additional deformation from the plane due to the flow of the coupling piece will not affect the kink assessment of the longitudinal stiffener and / or folds of the body.

However, this does not alter the fact that the joint of the pleat stiffener must be strengthened in order to flow appearance. The flow of the coupling piece will have an influence on the stiffness of the longitudinal stiffener against kinks and / or support against folds.

The testing of the connecting means is carried out in the Mathcad, see Appendix D8.c . This is based on of the voltages according to the linear calculation and a distinction is made in the upright flange and the body (= horizontal flange) of the longitudinal stiffener and the same parts of the coupling piece. From the Tensions in the different parts determine the forces on the rivets. From this calculation follows that the connection at section division S6 is not satisfactory, with a UC of 1.33, whereby butt of the rivet in the body (horizontal flange) of the coupling piece is decisive. Based on this UC can be derived that the allowable stress is 170 N / mm² / 1.33 = 127 N / mm². This would mean that the bottom connection at the location of C5 and C6 does not meet strength. The bottom stiffener on the spot of C4 (125 N / mm²) and C7 (129 N / mm²) are just on the edge, but by redistributing a small part it can be argued from the forces that this connection is sufficient.

Due to fatigue and the recently found noises in the connection, in consultation with Rijkswaterstaat, decided to replace all coupling pieces, despite the fact that they are calculated arithmetically meet. This will be further discussed in the reinforcement design.

Project related

5 Fatigue

5.1 Approach

The approach to the fatigue calculation is described in the basic report. In this chapter the results of the fatigue calculations are discussed. First of all, paragraph 5.2 deals with the stresses due to lateral bending and it is determined whether and if so how must be included in the fatigue calculations of the main beam. In paragraph 5.3 and In addition, an overview of the connection, the damage category and the results of fatigue damage calculation. The results are presented for $\gamma_{Mf} = 1.35$, both tabular and graphical. For $\gamma_{Mf} = 1.15$ and $\gamma_{Mf} = 1.0$ summaries of the results given at the beginning of the relevant appendices, including the report text somewhat compact.

For the main carriageway, the direction of travel changed in 1990. Therefore, for the HRB, the chosen the following approach. The damage development is calculated once with traffic direction Utrecht (indicated with "until 1989), and once with traffic to Germany (indicated with" from 1990). In both calculations, it is assumed (fictitiously) that the entire period (1964-2050) is being driven in the same direction. Then the damage is determined by the correct periods with the add the correct direction of travel.

- HRB west:
    - Damage period 1964-1989, calculation HRB west (until 1989, traffic towards Utrecht) +
    - Damage period 1990-2050, calculation HRB west (from 1990, traffic towards Germany)
- HRB east:
    - Damage period 1964-1989, calculation HRB east (until 1989, traffic towards Utrecht) +
    - Damage period 1990-2050, calculation HRB east (from 1990, traffic towards Germany)

5.2 Bending voltage change due to lateral bending

Using the local model, it was investigated how large the stresses in the lower flange of the main beam by laterally bending the bottom flange. Due to a load on the deck, the deck will want to bend between the main beams. This will cause an angular displacement at the top of the body of the main beam, which will push the bottom flanges outwards, see Figure 73 on the left. This one however, deformation is (locally) counteracted by the k-relationships.

Figure 73 - Lateral bending of the bottom flange (left) and rotation of the bridge (right)

Project related

In addition to lateral bending, the bridge will also rotate due to the eccentric load, see Figure 73 on the right. This will also cause the bottom flange to curve slightly, because this deformation at the location of the impositions are stopped.

To determine the magnitude of the stresses in the bottom flange by bending around the weak axis is one local model set up. For a description of the model, please refer to the principles report.

As boundary conditions, the deck on shaft 11 and shaft 14 is resilient in the longitudinal and transverse directions (x and y direction) supported, see Figure 74. In z-direction, there is a spring on the top of the body of the main beam support modeled on axis 11 and 14. The spring constants are derived from the global model by a unit load and the corresponding deformation of the relevant shaft on the shaft concerned determine points in the individual directions. The following spring stiffnesses follow from this.

Axis 11 k_x = 100 kN / m / 1.8 mm = 55.6 MN / mm^2
k_y = 100 kN / m / 7.6 mm = 13.2 MN / mm^2
k_z = 100 kN / 3.2 mm = 31 MN / m

Axis 14 k_x = 100 kN / m / 1.9 mm = 52.6 MN / mm^2
k_y = 100 kN / m / 9.1 mm = 11 MN / mm^2
k_z = 100 kN / 2.7 mm = 37 MN / m

Unit load Lane 1

Spring-loaded line support
(y)

Springy
imposition (z)

Springy
line lay-up (x)

Figure 74 - Local model with support conditions for the determination of stresses by transverse bending

Page 83

Project related

A unit load of 2x50 kN has been placed across the deck in lane 1, with the wheels centered at 2.15 m are placed symmetrically with respect to the center of lane 1, based on figure A.1 of NEN 8701, The unit load has been moved across the model in 0.1 m increments. The results for lane 2 can be determined by reading the results in the least loaded main beam, taking into account with the direction of deflecting the bottom flange.

The figures below show the deformations in the cross section with an axle load exactly between 2 k-bandages in (5 th crossbeam). The deformations show that the construction rotates slightly. This behavior matches the behavior in the global model.

Figure 75 - 3D deformation local model at unit load on 5 th cross beam (3D overview)

Page 84

Project related

It can also be seen that due to the bending of the cross beam / deck, the consoles pop up and the body of the main beam. This causes the bottom flange to rotate locally.

Figure 76 - 3D deformation local model at unit load on 5 th cross beam (deformation body and bottom flange)

In both figures below, the axle load is placed in the same location, exactly between 2 k-bandages (5 e

cross beam). The top figure shows the displacement of the crossbeam with k-bandage
(4 e cross-member), in the lower figure of the cross-member exactly in between the k-linkages in the (5 E
cross beam). The difference in deformation is a measure of the lateral deflection.

Figure 77 - 3D deformation of k-bandage at 4 th cross beam at unit load between 2 k-bandages in (5 th cross beam) (cross section)

Project related

Figure 78 - 3D deformation of cross beam between 2 k-braces in (5 th cross beam) with a unit load on the same cross beam (intersection)

The figure below shows the lateral deflection (u_y) of the bottom flange.

Figure 79 - Lateral deformation u_y lower flange at unit load between 2 k-bandages (5 th cross beam) (bottom view)

It can be seen that there is in particular a global curvature, due to the rotation of the cross section of the bridge. The local curvature between 2 k-relations as a result of the lateral deflection seems for the lower flange. It can also be seen that both main girders bend in the same direction. This means that a vehicle in lane 2 will produce an opposite side bend as one lane vehicle 1.

Project related

Tensions

The same picture can be seen in tensions in the bottom flange. The tensions are shown in the figure below shown in the bottom flange at a unit load between the 2 k-bandages. The difference in tension between the left and right side of the flange is very limited, only at the thickness transition there is one small disturbance visible. There is also a small disturbance when connecting the cross stiffeners visible, although less clear.

Figure 80 - Tensions in the bottom flange at unit load between 2 k-bandages in (5 th cross beam) (bottom view)

Lane 1

At 11 locations, the influence lines have been determined for the stresses due to transverse bending through traffic on lane 1. Because the model will also produce longitudinal bending, the stresses are transverse bending determined by determining the difference in tension between the left and right sides of the bottom flange and divide this by 2. This is then the occurring tensile and compressive stress in the extreme fiber of the lower flange due to M_z. The cuts are chosen so that they are not in the first half of the the first field and the second half of the last field are related to edge disturbances by the bearing conditions of the calculation model. The cuts are also chosen to be as minimal as possible are disturbed by the connections of the vertical stiffeners to the bottom flange and thickness transitions in the bottom flange.

Project related

The maximum transverse bending stresses during the passage of the unit load are in graph below. A distinction is made between the maximum voltage that occurs during the change (blue values) and the voltage when the axis is exactly above the considered cut condition (orange values). Because the voltage increases due to N + My, it will determining the total change the voltage due to Mz that occurs when the axis is exactly above the considered cut condition (orange values) are decisive and must be added to the voltage due to N + My. The vertical lines in the graph correspond to the position of the K-relationships.

Figure 81 - Tensions due to transverse bending

It should be noted that three different dimensions of the bottom flange can be distinguished in it considered piece. In cut 1 to 4 there is a plate of 500x20 mm in the bottom flange, in cut 5 to 7 a plate of 500x30 mm and in cuts 8 to 10 a plate of 500x30 mm + 550x30 mm. Because of this the tensions cannot be compared one-to-one.

The maximum transverse bending stresses to be added to the N + My stresses are the voltages indicated in orange, as these act as the axle load at the considered cut state. At approx. 67 m the maximum stress of ca σ_{Mz} = 0.5 N / mm² occurs . The tension in this cut due to the global behavior (N + My) under a unit load of 2x50 kN is 15 N / mm². The increase of the transverse bending stress is only 3%. Based on this small increase, it is global calculation model found sufficiently accurate that no correction needs to be applied to the voltages for verification of the main supporting structure for strength and fatigue. Moreover, the something falls higher stress due to transverse bending away against the overestimation of the stresses by the neglecting the longitudinal stiffeners in the cross-section properties in the global calculation model.

Project related

Lane 2

Measurements by TNO have shown that tensions due to lateral deflection as a result of traffic in lane 2 are somewhat larger in percentage than for lane 1. Therefore, in the same location as where the

measurements have been carried out (section 3), the voltage fluctuations due to traffic in lane 2 have also been determined.

Figure 82 - Tensions due to transverse bending at cut 3

This results in a stress due to transverse bending of ca σ_{Mz} = 0.35 N / mm². The change from longitudinal bending (N + My) is 5.38 N / mm2. The influence of transverse bending is therefore approximately 0.33 N / mm2 / 5.38 N / mm2 = 6%. Such as previously mentioned, the tension due to transverse bending by traffic in lane 2 works opposite to the tension due to traffic in lane 1, because rotation of the bridge prevails. This will mainly play in the middle of the spans and a little less at the supports.

Because the effect of traffic on lane 2 for the different beams works differently, below is made an assessment of the effect per beam.

Parallel carriageway west (most heavily loaded beam)
- The influence of transverse bending of traffic on lane 1 is very limited (3%)
- The influence of transverse bending of traffic on lanes 1 and 2 is opposite (favorable)

Parallel carriageway east (lightest loaded beam)
- The influence of transverse bending of traffic on lane 1 is slightly less limited than for the western beam, but still small (6%)
- The influence of transverse bending of traffic on lanes 1 and 2 is opposite (favorable)
- For the eastern beam, 61% of the total damage is caused by a vehicle on lane 1 and 2 together and 39% by a vehicle in lane 1
- Taking a very short turn means that the influence on the damage number of transverse bending is approx. 61% + 1.06 ^ 3 * 39% = 107%.

Main carriageway
- The main carriageway has a combination of the above, by changing the direction of travel, thus the effect remains small

TNO's measurements also show that the stresses due to longitudinal bending (N + My) in traffic are increasing lane 2 may be overestimated by the model. The tensions in traffic on lane 2 appear in the measurements are between 1.12 and 1.27 times lower than predicted by the local model. For lane 1 it appears that the tensions due to longitudinal bending match fairly well. The overestimation of the tensions in the model for traffic in lane 2 more than compensate for the (minor) effects of the transverse bend in traffic on the same lane. It was therefore decided to consider the influence of transverse bending not to be included in the calculation.

5.3 Type A: Weld end on bottom plate flange of main girder

The bottom flange of the main beam is reinforced with a reinforcement plate at various locations. The cover plate is connected to the bottom flange with a fillet weld of 5 mm. The top plate is tapered at the end tapering with usually a right angle. The most critical crack location is the welding stone at the continuous flange on the top side of the connection (see Figure 83) .

Figure 83 - The overview of the connection with critical crack location (not to scale) [R11499].

This connection occurs per 10 main beams at 10 different locations of the main bridge, so a total of 40 locations. Because of symmetry, for each main girder location A1 / A5 m tested, see Figure 84 t / m Figure 86 .

Figure 84 - Location of the connection type A - H in the 1 st field

Figure 85 - Location of the connection type A - H in the 2 nd field

Project related

Figure 86 - Location of the connection type A - H in the 3 rd field

The detail category for the fatigue calculation of this compound has been determined by TNO using the 'hot spot stress interpolation' method determined for the bridge as $\Delta\sigma_c = 58$ N / mm ^{2} where the buckling point of the SN curve is at 10^7. In accordance with report R11499, the main bridge may be assumed same category.

Figure 87 - Detail category for the fatigue calculation of the connection type 1 (bridge) and type A (main bridge)

A repair proposal has been determined by TNO for A5 in the western beam of the main carriageway (HRB). After the reinforcement has this detail in a detail category 75.4. This new detail category is based on Hobbacher's IIW recommendations [10] stating that the detail category is a factor of 1.3 increases after burr grinding. This calculation is according to TNO memorandum 0100313038-A / VSS [5] conservative, since the expansion of the weld with the 1/3 slope has not yet been taken into account. By performing the repair, the arithmetic fatigue damage is reduced to zero.

The calculation is for the 5 locations (A1 to A5) for 3 different safety factors $\gamma_{Mf} = 1.35$, 1.15 and 1.00 performed. The test results (damage numbers) are determined in the individual main beams, namely for the main carriageway west (HRB west), the main carriageway east (HRB east), the parallel carriageway west (PRB-West) and the parallel carriageway-East (PRB-East), because for each main girder they are different be burdened. For A5 in HRB West, a calculation was made of the situation before (A5) and after amplification (A5 rep).

Project related

Table 35 shows the results for $\gamma_{Mf} = 1.35$. The test results with the other safety factors are shown in Appendix E1 . Most compounds are found not to meet the damage requirement D <1.0 at $\gamma_{Mf} = 1.35$. This also applies to the repaired connection. This will no longer apply in 2036 meets the damage requirement, in accordance with the year stated in TNO memo [0100313038-A / VSS] 2036.

γ_{Mf} =								
1.35	**HRB west**		**HRB east**		**PRB west**		**PRB east**	
	2018	**2050**	**2018**	**2050**	**2018**	**2050**	**2018**	**2050**
A1	3.1	10.5	1.7	2.2	3.1	6.8	0.2	0.4
A2	2.5	8.4	1.6	2.0	2.6	5.5	0.2	0.3
A3	4.9	15.4	3.2	5.4	4.6	9.9	0.9	2.0
A4	1.0	3.5	0.5	0.6	1.0	2.3	0.0	0.0
A5	2.6	8.3	1.5	2.3	2.5	5.4	0.3	0.7
A5 (rep)		2.1						

Table 35 - Damage numbers of connection type A for the end of 2018 and the end of 2050 ($\gamma_{Mf} = 1.35$)

Figure 88 - Presentation of damage numbers for the first half of the bridge before 2050 ($\gamma_{Mf} = 1.35$) (for repair)

Project related

5.4 Type B: Flange spacers at the level of the rivet in section division

The main bridge is divided into a number of sections. At the location of these section divisions is the bottom flange widens by welding on an extra plate (flange widener). The flange wideners have different sizes and occur a total of 16 times per main beam.

Figure 89 - Photo of the compound [R11499].

Figure 90 - Overview of the connection with critical crack location

Because of symmetry, only the first 8 details e (B1 to B8). For the locations reference is made to Figures 84 to 86.

The detail category was determined by TNO using the 'hot spot voltage interpolation' method, see report [R11499], and depends on the presence of a transverse stiffener in the area of influence of the welded joint at the end of the flange widener. For the details with a cross stiffener applies detail category 40 (B2, B4 and B7). For the other details, category 46 applies. The kink point of the SN curve is at 10_{7} .

Figure 91 - Detail category for the fatigue calculation of the type B connection

NB: The analysis by TNO assumes that there is a weld between the end face of the extender and the through flange. This assumption has been verified by Rijkswaterstaat / Infra Inspection,

which means that the category retained can be used by TNO.

For B4 and B7, a repair proposal has been determined by TNO for the western beam of the main carriageway [0100313038-A / VSS]. After the amplification, this detail has a detail category 100, because there is a smooth one transition is created. As a result, only a longitudinal weld remains, which in accordance with table 8.1 from the NEN EN 1993-1-9 may be used as category 100. By performing the repair, the arithmetic fatigue damage reduced to zero.

The calculation is for the 8 locations (B1 to B8) for 3 different safety factors γ_{Mf} = 1.35, 1.15 and 1.00 performed. For B4 and B7 of HRB West, a calculation has been made of the situation before (B4 / B7) and after reinforcement (B4 rep / B7 rep).

Project related

Table 35 shows the results for γ_{Mf} = 1.35. The test results with the other safety factors are shown in Appendix E2 . Most compounds are found not to meet the damage requirement D <1.0 at γ_{Mf} = 1.35. This also applies to the repaired compound B4. At the end of 2032, this no longer meets the damage claim. This is virtually the same as the year 2034 stated in the TNO memo [0100313038-A / VSS].

γ_{Mf} = 1.35 HRB west			HRB east		PRB west		PRB east	
	2018	2050	2018	2050	2018	2050	2018	2050
B1	6.2	20.4	3.5	4.5	6.3	13.4	0.4	0.8
B2	7.7	24.7	5.1	6.6	7.8	16.3	0.6	1.4
B3	2.8	9.1	1.4	1.8	2.9	6.0	0.1	0.3
B4	26.2	81.3	16.9	27.4	25.1	52.6	4.6	9.8
B5	1.6	5.0	1.1	2.1	1.4	3.1	0.4	0.9
B6	1.6	5.3	0.9	1.0	1.6	3.4	0.0	0.1
B7	8.3	25.9	5.6	9.2	7.9	16.6	1.5	3.4
B8	5.0	16.1	3.0	4.3	4.9	10.5	0.5	1.1
B4 (rep)		2.8						
B7 (rep)		0.5						

Table 36 - Damage numbers of connection type B for the end of 2018 and the end of 2050 (γ_{Mf} = 1.35)

Figure 92 - Presentation of damage numbers for the first half of the bridge before 2050 (γ_{Mf} = 1.35) (for repair)

Project related

5.5 Type C: Riveted joints bridge sections

The main bridge is divided into a number of sections. Locate these section divisions rivet joints applied in the main beam. In total there are 16 section divisions per main bea because of symmetry, C1 to C8 have been tested, see Figures 84 to Figure 86.

Figure 93 - Bottom view of bottom flange [Drawing A.85383 / A.85365 / A.85366]

The detail category $\Delta\sigma_c$ for the fatigue calculation of this connection follows from the RBK and amounts to 80 N / mm ^{2} . For the slope of the first branch of SN curve (m_1), 5 is used in accordance with the RBK. The stresses are determined on the underside of the flange, based on the net cross section of the bottom flange, but including the flange widener. This is based on a cut with four holes in the bottom flange. The properties of the (net) cross-section properties have been determined with SCIA.

Figure 94 - Detail category for the fatigue calculation of the type C connection

The calculation is for the 8 locations (C1 to C8) for 3 different safety factors γ_{Mf} = 1.35, 1.15 and 1.00 executed. The test results (damage numbers) are determined in the individual main beams, namely for the main carriageway west (HRB west), the main carriageway east (HRB east), the parallel carriageway west (PRB-West) and the parallel carriageway-East (PRB-East).

Page 96

Project related

Bottom flange

Table 37 and Fi ır γ_{Mf} = 1.35 for the rivet joint in the bottom flange. The test results with the other safety factors are shown in Appendix E3. Approx 40% of the compounds appear not to meet the damage requirement D <1.0 at γ_{Mf} = 1.35. The most critical connection is located at C4 in the main carriageway west. The damage at the end of 2050 is 7.5 here.

γ_{Mf} = 1.35	HRB west		HRB east		PRB west		PRB east	
	2018	2050	2018	2050	2018	2050	2018	2050
C1	0.4	1.6	0.1	0.2	0.3	0.9	0.0	0.0
C2	0.3	1.1	0.1	0.2	0.2	0.7	0.0	0.0
C3	0.1	0.3	0.0	0.0	0.1	0.2	0.0	0.0
C4	1.9	7.5	0.9	1.5	1.7	4.5	0.1	0.4
C5	0.0	0.2	0.0	0.0	0.0	0.1	0.0	0.0
C6	0.0	0.1	0.0	0.0	0.0	0.1	0.0	0.0

C7	0.2	1.0	0.1	0.2	0.2	0.6	0.0	0.1
C8	0.4	1.6	0.2	0.2	0.4	1.0	0.0	0.1

Table 37 - Damage figures for connection type C (bottom flange) for the end of 2018 and the end of 2050 ($\gamma_{Mf} = 1.35$)

Figure 95 - Presentation of damage numbers (bottom flange) for the first half of the bridge by 2050 ($\gamma_{Mf} = 1.35$)

Project related

Top flange

Table 38 shows the results for $\gamma_{Mf} = 1.35$ for the top flange rivet joint. The test results with the other safety factors are shown in Appendix E3 . All damage numbers are equal to 0.0 at $\gamma_{Mf} = 1.35$, because the tension in the top flange is considerably lower compared to the bottom flange.

$\gamma_{Mf} = 1.35$	HRB west		HRB east		PRB west		PRB east	
	2018	2050	2018	2050	2018	2050	2018	2050
C1	0.0	0.0	0.0	0.0	0.0	0.0	0.0	0.0

C2	0.0	0.0	0.0	0.0	0.0	0.0	0.0	0.0
C3	0.0	0.0	0.0	0.0	0.0	0.0	0.0	0.0
C4	0.0	0.0	0.0	0.0	0.0	0.0	0.0	0.0
C5	0.0	0.0	0.0	0.0	0.0	0.0	0.0	0.0
C6	0.0	0.0	0.0	0.0	0.0	0.0	0.0	0.0
C7	0.0	0.0	0.0	0.0	0.0	0.0	0.0	0.0
C8	0.0	0.0	0.0	0.0	0.0	0.0	0.0	0.0

Table 38 - Damage numbers of connection type C (top flange) for the end of 2018 and the end of 2050 ($\gamma_{Mf} = 1.35$)

Body

For connections C4 and C8, the damage in the bottom rows of rivets in the body was examined. This one cuts had the highest damage rates when testing the bottom flange. Because the tension decreases on the height of the body, rows 1, 3, 5, 6 and 7 have been tested for connection C4, seen from the bottom flange. Only row 1 has been tested for C8.

γ_{Mf} **= 1.35 HRB west**			**HRB east**		**PRB west**		**PRB east**	
	2018	**2050**	**2018**	**2050**	**2018**	**2050**	**2018**	**2050**
C4 body row 1	1.4	5.5	0.7	1.1	1.3	3.3	0.1	0.3
C4 body row 3	0.8	3.2	0.4	0.6	0.7	2.0	0.1	0.2
C4 body row 5	0.5	1.8	0.2	0.3	0.4	1.1	0.0	0.1
C4 body row 6	0.3	1.3	0.1	0.2	0.3	0.7	0.0	0.1
C4 body row 7	0.2	0.8	0.1	0.1	0.2	0.5	0.0	0.0
C8 row 1 body	0.2	1.0	0.1	0.1	0.2	0.6	0.0	0.0

Table 39 - Damage numbers of connection type C (body) for the end of 2018 and the end of 2050 ($\gamma_{Mf} = 1.35$)

In the body of junction C4, in the western main girder of the main carriageway, rows 1 to 6 of the rivets, seen from below, do not meet the damage requirement D <1.0 at $\gamma_{Mf} = 1.35$. From the western rows 1 to 5 do not meet the main beam of the parallel carriageway. The eastern beams are satisfactory throughout height of the body. Also in connection C8, the rivets in the body meet the damage requirement.

Project related

5.6 Type D: Internal cross stiffener - main beam flange

A vertical transverse stiffener is applied to the body of the main beam with each cross beam. The

stiffener is connected to the bottom flange of the main beam with a ½ V weld of 10 mm. The critical crack location is the toe of the weld on the flange of the end face of the joint, with red indicated in Figure 96 . The throat size of the weld is assumed to be 4 mm, but according to TNO actually a negligible influence on the voltage intensity.

167 transverse stiffeners were used per main beam. Of these, the positions at the location of the K-relationships and portals of the half bridge tested (D1 to D30); see Figure 97 through Figure 99.

Figure 96 - Detail vertical pleat stiffener - flange connection [A.85317]

Figure 97 - Location of the connection type D - G and I - K in the 1 st field

Figure 98 - Location of the connection type D - G and I - K in the 2 nd field

Figure 99 - Location of the compound of type D - G I - K in the third E field

The detail category for the fatigue calculation of this compound has been determined by TNO using the hot spot stress interpolation method determined as $\Delta\sigma_c = 69$ N / mm ^{2} .

Figure 100 - Detail category for the fatigue calculation of the type D connection

The calculation is for the 30 locations (D1 to D30) for 3 different safety factors $\gamma_{Mf} = 1.35$, 1.15 and 1.00 executed. The test results (damage numbers) are determined in the individual main beams, namely for the main carriageway west (HRB west), the main carriageway east (HRB east), the parallel carriageway west (PRB-West) and the parallel carriageway-East (PRB-East).

Project related

Table 40 and F $\gamma_{Mf} = 1.35$. The test results with the other safety factors are in Appendix B4. displayed. About 40% of the connections turned out to be unsatisfactory to the claim D <1.0 at $\gamma_{Mf} = 1.35$. The most critical connection is at D13 (middle 2nd field) in the main carriageway west. The damage in 2050 is 11.3 here.

$\gamma_{Mf} = 1.35$	HRB west		HRB east		PRB west		PRB east	
	2018	2050	2018	2050	2018	2050	2018	2050
D1	0.0	0.0	0.0	0.0	0.0	0.0	0.0	0.0
D2	0.3	1.2	0.1	0.1	0.3	0.8	0.0	0.0
D3	0.6	2.3	0.3	0.3	0.5	1.4	0.0	0.0
D4	1.3	4.5	0.7	0.8	1.2	2.9	0.0	0.1
D5	1.5	5.1	0.7	0.9	1.4	3.2	0.0	0.1
D6	1.4	4.9	0.8	1.0	1.4	3.1	0.0	0.1
D7	0.9	3.3	0.5	0.7	0.9	2.1	0.0	0.1
D8	1.1	4.0	0.7	0.9	1.1	2.5	0.0	0.1
D9	0.4	1.3	0.2	0.3	0.3	0.8	0.0	0.1
D10	1.7	5.8	0.9	1.3	1.7	3.7	0.1	0.2
D11	0.8	2.7	0.3	0.4	0.8	1.8	0.0	0.0
D12	2.3	7.6	1.1	1.4	2.3	4.9	0.1	0.3
D13	3.5	11.3	1.9	2.9	3.4	7.3	0.4	0.8
D14	2.8	9.3	1.6	2.6	2.7	5.9	0.4	0.9
D15	0.5	2.0	0.3	0.5	0.5	1.2	0.1	0.1
D16	0.5	1.8	0.3	0.5	0.5	1.1	0.1	0.2
D17	0.3	1.1	0.2	0.3	0.2	0.7	0.0	0.1
D18	0.1	0.5	0.1	0.1	0.1	0.3	0.0	0.1
D19	0.0	0.2	0.0	0.0	0.0	0.1	0.0	0.0
D20	0.2	0.8	0.1	0.1	0.2	0.5	0.0	0.0
D21	0.1	0.3	0.0	0.0	0.1	0.2	0.0	0.0
D22	0.2	0.8	0.1	0.1	0.2	0.5	0.0	0.0
D23	0.1	0.6	0.1	0.1	0.1	0.4	0.0	0.0
D24	0.4	1.4	0.2	0.3	0.4	0.9	0.0	0.1
D25	0.8	2.9	0.5	0.7	0.8	1.8	0.1	0.2
D26	0.7	2.3	0.3	0.5	0.6	1.5	0.0	0.1
D27	0.5	1.8	0.2	0.3	0.5	1.1	0.0	0.1
D28	0.9	3.0	0.4	0.6	0.8	1.9	0.0	0.1
D29	1.2	4.1	0.6	0.8	1.1	2.6	0.1	0.2
D30	1.3	4.7	0.7	1.0	1.3	3.0	0.1	0.2

Table 40 - Damage numbers of compound type D for the end of 2018 and the end of 2050 ($\gamma_{Mf} = 1.35$)

Page 101

Project related

Figure 101 - Presentation of damage numbers for the first half of the bridge before 2050 ($\gamma_{Mf} = 1.35$)

5.7 Type E: Cross stiffener inside - main beam body

A vertical transverse stiffener is applied to the body of the main beam with each cross beam. The stiffener is connected to the body of the main beam with a 4 mm weld. Per main beam are 167 cross stiffeners applied. Of these, the positions at the K - bonds and portals of the half bridge tested (E1 to E30); see Figure 97 through Figure 99.

Figure 102 - Detail of vertical pleat stiffener - web connection [A.85362-A.85367 / A.85377]

The detail category for the fatigue calculation of this compound has been determined by TNO using the hot spot stress interpolation method determined as $\Delta\sigma_c = 80$ N / mm ^{2} .

Figure 103 - Detail category for the fatigue calculation of the type E connection

The calculation is for the 30 locations (E1 to E30) for 3 different safety factors $\gamma_{Mf} = 1.35, 1.15$

and 1.00 executed. The test results (damage numbers) are determined in the individual main beams, namely for the main carriageway west (HRB west), the main carriageway east (HRB east), the parallel carriageway west (PRB-West) and the parallel carriageway-East (PRB-East).

Project related

Table 41 and Fi $\gamma_{Mf} = 1.35$. The test results with the other safety factors are snown in Appendix E5. About 25% of the connections turned out to be unsatisfactory to the claim D <1.0 at $\gamma_{Mf} = 1.35$. The most critical connection is at E13 (center field 2) in the main carriageway west. The damage in 2050 is 6.7 here.

γ_{Mf} = 1.35 HRB west			HRB east		PRB west		PRB east	
	2018	2050	2018	2050	2018	2050	2018	2050
E1	0.0	0.0	0.0	0.0	0.0	0.0	0.0	0.0
E2	0.1	0.5	0.0	0.0	0.1	0.3	0.0	0.0
E3	0.3	1.2	0.1	0.1	0.2	0.7	0.0	0.0
E4	0.7	2.5	0.3	0.4	0.6	1.6	0.0	0.1
E5	0.8	2.9	0.4	0.5	0.8	1.8	0.0	0.1
E6	0.8	2.7	0.4	0.5	0.7	1.7	0.0	0.1
E7	0.5	1.8	0.3	0.3	0.5	1.1	0.0	0.0
E8	0.6	2.2	0.4	0.4	0.6	1.4	0.0	0.1
E9	0.2	0.6	0.1	0.1	0.1	0.4	0.0	0.0
E10	1.0	3.4	0.5	0.7	0.9	2.1	0.0	0.1
E11	0.4	1.4	0.1	0.2	0.4	0.9	0.0	0.0
E12	1.3	4.4	0.6	0.8	1.3	2.8	0.0	0.1
E13	2.0	6.7	1.1	1.6	2.0	4.3	0.2	0.4
E14	1.6	5.4	0.9	1.5	1.5	3.4	0.2	0.4
E15	0.2	1.0	0.1	0.2	0.2	0.6	0.0	0.1
E16	0.2	0.8	0.1	0.2	0.2	0.5	0.0	0.1
E17	0.1	0.5	0.1	0.1	0.1	0.3	0.0	0.0
E18	0.0	0.2	0.0	0.1	0.0	0.1	0.0	0.0
E19	0.0	0.1	0.0	0.0	0.0	0.0	0.0	0.0
E20	0.1	0.4	0.0	0.0	0.1	0.2	0.0	0.0
E21	0.0	0.1	0.0	0.0	0.0	0.1	0.0	0.0
E22	0.1	0.4	0.0	0.0	0.1	0.2	0.0	0.0
E23	0.1	0.3	0.0	0.0	0.1	0.2	0.0	0.0

E24	0.1	0.6	0.1	0.1	0.1	0.4	0.0	0.0
E25	0.4	1.5	0.2	0.3	0.4	0.9	0.0	0.1
E26	0.3	1.2	0.1	0.2	0.3	0.7	0.0	0.1
E27	0.2	0.9	0.1	0.1	0.2	0.5	0.0	0.0
E28	0.4	1.6	0.2	0.3	0.4	1.0	0.0	0.1
E29	0.6	2.3	0.3	0.4	0.6	1.4	0.0	0.1
E30	0.7	2.6	0.4	0.5	0.7	1.6	0.0	0.1

Table 41 - Damage numbers of connection type E for the end of 2018 and the end of 2050 ($\gamma_{Mf} = 1.35$)

Page 104

Project related

Figure 104 - Presentation of damage figures for the first half of the bridge before 2050 ($\gamma_{Mf} = 1.35$)

Project related

5.8 Type F: Cross stiffener outside - main beam flange

In addition to a transverse stiffener on the inside, every K-bandage also has a vertical transverse stiffener applied on the outside of the main spar web. The flange of the stiffener is on the outside connected to the bottom flange of the main beam with a 4 mm weld. Per main beam are 59 cross stiffeners applied. Of these, the positions at the K - links and the portals of tl half bridge tested (F1 to F30); see Figure 97 through Figure 99.

Figure 105 - Detail of vertical pleat stiffener - flange connection [A.85377]

The detail category for the fatigue calculation of this compound has been determined by TNO as $\Delta\sigma_c = 71$ N / mm ^{2} ; see [R11499, Appendix D Table 8.4, Detail 1].

Figure 106 - Detail category for the fatigue calculation of the type F connection

The calculation is for the 30 locations (F1 to F30) for 3 different safety factors $\gamma_{Mf} = 1.35$, 1.15 and 1.00 executed. The test results (damage numbers) are determined in the individual main beams, namely for the main carriageway west (HRB west), the main carriageway east (HRB east), the parallel carriageway west (PRB-West) and the parallel carriageway-East (PRB-East).

Project related

Figure 107 and Ta or $\gamma_{Mf} = 1.35$. The test results with the other safety factors are shown in Appendix E6. About 40% of the connections turned out to be unsatisfactory to the claim D <1.0 at $\gamma_{Mf} = 1.35$. The most critical connection is at F13 in the main carriageway west. The damage in 2050 is 10.3 here.

$\gamma_{Mf} = 1.35$	HRB west		HRB east		PRB west		PRB east	
	2018	2050	2018	2050	2018	2050	2018	2050
F1	0.0	0.0	0.0	0.0	0.0	0.0	0.0	0.0
F2	0.3	1.1	0.1	0.1	0.3	0.6	0.0	0.0
F3	0.5	2.0	0.2	0.3	0.5	1.2	0.0	0.0
F4	1.1	4.0	0.6	0.7	1.1	2.6	0.0	0.1
F5	1.3	4.5	0.7	0.8	1.3	2.9	0.0	0.1
F6	1.2	4.4	0.7	0.8	1.2	2.8	0.0	0.1
F7	0.8	3.0	0.5	0.6	0.8	1.9	0.0	0.1

F8	1.0	3.6	0.6	0.8	1.0	2.3	0.0	0.1
F9	0.3	1.2	0.2	0.3	0.3	0.7	0.0	0.1
F10	1.5	5.3	0.8	1.1	1.5	3.3	0.1	0.2
F11	0.7	2.4	0.3	0.3	0.7	1.6	0.0	0.0
F12	2.0	6.8	1.0	1.3	2.0	4.4	0.1	0.2
F13	3.1	10.3	1.7	2.6	3.0	6.6	0.3	0.8
F14	2.5	8.4	1.5	2.4	2.4	5.3	0.3	0.8
F15	0.5	1.8	0.2	0.4	0.4	1.1	0.0	0.1
F16	0.4	1.6	0.2	0.4	0.4	1.0	0.1	0.1
F17	0.2	0.9	0.1	0.3	0.2	0.6	0.0	0.1
F18	0.1	0.4	0.1	0.1	0.1	0.2	0.0	0.0
F19	0.0	0.1	0.0	0.0	0.0	0.1	0.0	0.0
F20	0.2	0.7	0.1	0.1	0.1	0.4	0.0	0.0
F21	0.1	0.3	0.0	0.0	0.1	0.2	0.0	0.0
F22	0.2	0.7	0.1	0.1	0.1	0.4	0.0	0.0
F23	0.1	0.5	0.1	0.1	0.1	0.3	0.0	0.0
F24	0.3	1.2	0.2	0.2	0.3	0.7	0.0	0.0
F25	0.7	2.6	0.4	0.7	0.7	1.6	0.1	0.2
F26	0.6	2.1	0.3	0.4	0.5	1.3	0.0	0.1
F27	0.4	1.6	0.2	0.3	0.4	1.0	0.0	0.1
F28	0.8	2.7	0.4	0.5	0.7	1.7	0.0	0.1
F29	1.0	3.7	0.5	0.7	1.0	2.3	0.1	0.2
F30	1.2	4.2	0.6	0.9	1.2	2.7	0.1	0.2

Table 42 - Damage numbers of connection type F for the end of 2018 and the end of 2050 ($\gamma_{Mf} = 1.35$)

Figure 107 - Presentation of damage numbers for the first half of the bridge before 2050 (γ_{Mf} = 1.35)

Project related

5.9 Type G: x-seam bottom beam main beam

The bottom flange of the main beam is fitted with reinforcement plates. Where these plates continue they are welded together with a x seams in the bottom flange per main beam,

see Figure 109 to Figu some details almost coincides, one of them
number of locations gr G1 to G12 were tested.

Figure 108 - Bottom flange weld joint detail [Source: A.85366]

Figure 109 - Location of the connection type G in the 1 st field

Figure 110 - Location of the type G connection in the 2 nd field

Figure 111 - Location of the connection type G in the 3 rd field

The detail category $\Delta\sigma_c$ for the fatigue calculation of this connection follows from NEN-EN 1993-1-9 table 8.3 Detail 5 and amounts to 90 N / mm ^{2} . For compound G1, G2, G6, G7, G8 and G12, a factor $k_s = (25/30)^{0.2} = 0.96$ charged. For the other connections, the thickness of the thickening plate is smaller than 25mm so that the factor k_s equals 1.0.

Figure 112 - Detail category for the fatigue calculation of the type G connection

The calculation is for the 12 locations (G1 to G12) for 3 different safety factors $\gamma_{Mf} = 1.35, 1.15$ and 1.00 executed. The test results (damage numbers) are determined in the individual main beams, namely for the main carriageway west (HRB west), the main carriageway east (HRB east), the parallel carriageway west (PRB-West) and the parallel carriageway-East (PRB-East).

Project related

Table 43 and Fi $\gamma_{Mf} = 1.35$. The test results with the other safety factors are shown in Appendix E7. About 25% of the connections turned out to be unsatisfactory to the claim D <1.0 at $\gamma_{Mf} = 1.35$. The most critical connection is at G5 in the main carriageway west. The damage in 2050 is 3.5 here.

γ_{Mf} = 1.35 HRB west			HRB east		PRB west		PRB east	
	2018	2050	2018	2050	2018	2050	2018	2050
G1	0.4	1.6	0.2	0.2	0.4	1.0	0.0	0.0
G2	0.4	1.3	0.2	0.2	0.3	0.8	0.0	0.0
G3	0.6	2.0	0.3	0.4	0.5	1.3	0.0	0.0
G4	0.8	2.9	0.4	0.5	0.8	1.8	0.0	0.1
G5	1.0	3.5	0.5	0.8	0.9	2.2	0.1	0.2
G6	0.1	0.6	0.1	0.1	0.1	0.3	0.0	0.0
G7	0.0	0.0	0.0	0.0	0.0	0.0	0.0	0.0
G8	0.0	0.1	0.0	0.0	0.0	0.1	0.0	0.0
G9	0.1	0.3	0.0	0.0	0.1	0.2	0.0	0.0
G10	0.1	0.3	0.0	0.0	0.1	0.2	0.0	0.0
G11	0.4	1.3	0.1	0.2	0.3	0.8	0.0	0.1
G12	0.5	1.8	0.2	0.3	0.5	1.1	0.0	0.1

Table 43 - Damage numbers of connection type G for the end of 2018 and the end of 2050 ($\gamma_{Mf} = 1.35$) (DC = 90)

Figure 113 - Presentation of damage numbers for the first half of the bridge before 2050 ($\gamma_{Mf} = 1.35$)

Project related

For the inaccessible sides of the x-welds that are between the plates, this applies in the past are ground flat. A higher detail category can be used for this, namely the detail category 112, in accordance with detail 1 of table 8.3.

.

Figure 114 - Detail category for the fatigue calculation of the connection type G (flat ground side)

Distinguishing between the flat-ground weld and the non-ground-ground weld is possible advantages in determining the reinforcements, because the flat-ground side is more difficult / impossible to reach. The damage numbers are shown in the table below for $\gamma_{Mf} = 1.35$. This has been taken into account with the thickness of the plate, as described under Figure 107.

$\gamma_{Mf} = 1.35$ HRB west			HRB east		PRB west		PRB east	
	2018	2050	2018	2050	2018	2050	2018	2050
G1	0.1	0.5	0.0	0.1	0.1	0.3	0.0	0.0
G2	0.1	0.4	0.0	0.1	0.1	0.2	0.0	0.0
G3	0.2	0.7	0.1	0.1	0.1	0.4	0.0	0.0
G4	0.3	1.1	0.1	0.1	0.2	0.6	0.0	0.0
G5	0.4	1.4	0.2	0.3	0.3	0.8	0.0	0.1
G6	0.0	0.2	0.0	0.0	0.0	0.1	0.0	0.0
G7	0.0	0.0	0.0	0.0	0.0	0.0	0.0	0.0
G8	0.0	0.0	0.0	0.0	0.0	0.0	0.0	0.0
G9	0.0	0.1	0.0	0.0	0.0	0.0	0.0	0.0
G10	0.0	0.1	0.0	0.0	0.0	0.0	0.0	0.0
G11	0.1	0.4	0.0	0.1	0.1	0.2	0.0	0.0
G12	0.1	0.6	0.1	0.1	0.1	0.3	0.0	0.0

Table 44 - Damage numbers of connection type G for the end of 2018 and the end of 2050 ($\gamma_{Mf} = 1.35$) (DC = 112)

Project related

5.10 Type H: Flange widener at the height of supports

At the location of the supports, the bottom flange of the main beam is fitted with a flange widener. This spacer occurs a total of 6 tim symmetry, only H1 to H3 are tested. see Figure 84 to Figure 86

Support A [A.85373] *Support B [A.85374]* *Support C [A.85375]*

Figure 115 - Detail of flange flange supports

The detail category for the fatigue calculation of this compound has been determined by TNO using the hot spot stress interpolation method determined as $\Delta\sigma_c = 46$ N / mm ^{2} ; see TNO report [R11499 table 5.3], according to type B.

The calculation is for the 3 locations (H1 to H3) for 3 different safety factors $\gamma_{Mf} = 1.35$, 1.15 and 1.00 executed. The test results (damage numbers) are determined in the individual main beams, namely for the main carriageway west (HRB west), the main carriageway east (HRB east), the parallel carriageway west (PRB-West) and the parallel carriageway-East (PRB-East).

Table 45 and Fi $\gamma_{Mf} = 1.35$. The test results with the other safety factors are shown in Appendix E8. Most connections at the intermediate supports appear not to meet the damage requirement D <1.0 at $\gamma_{Mf} = 1.35$. The most critical the connection is located at H2 in the main carriageway west. The damage in 2050 is 23.3 here.

$\gamma_{Mf} = 1.35$	HRB west		HRB east		PRB west		PRB east	
	2018	2050	2018	2050	2018	2050	2018	2050

H1	0.0	0.0	0.0	0.0	0.0	0.0	0.0	0.0
H2	7.2	23.3	4.4	6.1	7.1	15.1	0.7	1.5
H3	1.5	5.2	0.8	0.9	1.5	3.4	0.0	0.1

Table 45 - Damage numbers of connection type H for the end of 2018 and the end of 2050 (γ_{Mf} = 1.35)

Figure 116 - Presentation of damage numbers for the first half of the bridge before 2050 (γ_{Mf} = 1.35)

5.11 Type I: Cross stiffener outside - main beam body

Each K-bandage has a vertical transverse stiffener on the outside of the main beam body on the outside applied. The body of this vertical stiffener is attached to the main beam body with a 4 mm weld welded. 59 cross stiffeners were used per main beam. Due to symmetry, these are the positions tested over the first half of the bridge (I1 to I30); see Figure 97 through Figure 99.

Figure 117 - Weld detail between stiffener body and main beam body [A.85377]

The detail category for the fatigue calculation of this compound has been determined by TNO as $\Delta\sigma_c$ = 80 N / mm 2 ; see [R11499, Appendix D Table 8.4, Detail 7].

Figure 118 - Detail category for the fatigue calculation of the type I connection

The locations and detail category of type I is the same as type E. Therefore, for the fatigue calculation refer to H5. 7. The results have been reproduced for completeness.

Project related

Table 46 and Figure 119 show the results for γ_{Mf} = 1.35. The test results with the other safety factors are shown in Appendix E9. About 40% of the connections turned out to be unsatisfactory to the claim D <1.0 at γ_{Mf} = 1.35. The most critical connection is at I13 in the main carriageway west. The damage in 2050 is 6.7 here.

γ_{Mf} = 1.35	HRB west		HRB east		PRB west		PRB east	
	2018	2050	2018	2050	2018	2050	2018	2050
I1	0.0	0.0	0.0	0.0	0.0	0.0	0.0	0.0
I2	0.1	0.5	0.0	0.0	0.1	0.3	0.0	0.0
I3	0.3	1.2	0.1	0.1	0.2	0.7	0.0	0.0
I4	0.7	2.5	0.3	0.4	0.6	1.6	0.0	0.1
I5	0.8	2.9	0.4	0.5	0.8	1.8	0.0	0.1
I6	0.8	2.7	0.4	0.5	0.7	1.7	0.0	0.1
I7	0.5	1.8	0.3	0.3	0.5	1.1	0.0	0.0
I8	0.6	2.2	0.4	0.4	0.6	1.4	0.0	0.1
I9	0.2	0.6	0.1	0.1	0.1	0.4	0.0	0.0
I10	1.0	3.4	0.5	0.7	0.9	2.1	0.0	0.1
I11	0.4	1.4	0.1	0.2	0.4	0.9	0.0	0.0
I12	1.3	4.4	0.6	0.8	1.3	2.8	0.0	0.1
I13	2.0	6.7	1.1	1.6	2.0	4.3	0.2	0.4

I14	1.6	5.4	0.9	1.5	1.5	3.4	0.2	0.4
I15	0.2	1.0	0.1	0.2	0.2	0.6	0.0	0.1
I16	0.2	0.8	0.1	0.2	0.2	0.5	0.0	0.1
I17	0.1	0.5	0.1	0.1	0.1	0.3	0.0	0.0
I18	0.0	0.2	0.0	0.1	0.0	0.1	0.0	0.0
I19	0.0	0.1	0.0	0.0	0.0	0.0	0.0	0.0
I20	0.1	0.4	0.0	0.0	0.1	0.2	0.0	0.0
I21	0.0	0.1	0.0	0.0	0.0	0.1	0.0	0.0
I22	0.1	0.4	0.0	0.0	0.1	0.2	0.0	0.0
I23	0.1	0.3	0.0	0.0	0.1	0.2	0.0	0.0
I24	0.1	0.6	0.1	0.1	0.1	0.4	0.0	0.0
I25	0.4	1.5	0.2	0.3	0.4	0.9	0.0	0.1
I26	0.3	1.2	0.1	0.2	0.3	0.7	0.0	0.1
I27	0.2	0.9	0.1	0.1	0.2	0.5	0.0	0.0
I28	0.4	1.6	0.2	0.3	0.4	1.0	0.0	0.1
I29	0.6	2.3	0.3	0.4	0.6	1.4	0.0	0.1
I30	0.7	2.6	0.4	0.5	0.7	1.6	0.0	0.1

Table 46 - Damage figures for compound type I for the end of 2018 and the end of 2050 ($\gamma_{Mf} = 1.35$)